MODELING AND CONTROL OF HIGH DENSITY MICROCANTILEVER SYSTEMS

BY

BERKEM MEHMET

THESIS

Submitted in partial fulfillment of the requirements
for the degree of Master of Science in Mechanical Engineering
in the Graduate College of the
University of Illinois at Urbana-Champaign, 2012

Urbana, Illinois

Adviser:

Professor Petros Voulgaris

ABSTRACT

In this thesis we build on our earlier work on the control of high density, electrostatically actuated, microcantilever arrays and present simple state feedback controllers that can achieve reasonable performance. These controllers are localized, spatially distributed and yield tracking performances comparable to the performance of the more complex H_∞ controller that takes disturbances and couplings into account, for reference frequencies as high as 3000 rad/sec. These simpler structures come with the cost of worse performance at higher frequencies, relatively inferior robustness to phase shifts and a state availability requirement. Therefore, they can be effectively used for relatively lower bandwidth applications where the states are measurable. The H_∞ controller on the other hand operates quite well at higher, spatially varying frequencies despite having a limited output information. This can be first demonstrated by developing a centralized controller for an array consisting of a finite number of cantilevers in order to have a benchmark. Using infinite abstraction methods however a localized and spatially distributed controller on par with the centralized control can be developed for the infinite cantilever array.

Instead of regarding only the cantilever tip as if the cantilever was a point mass the above results can be further verified by using a multimodal model of the cantilever system. The FEM model, as a typical multimodal method, views the cantilever as a more complex structure by cutting it into seg-

ments and taking the dynamics of each segment into calculation. Hence this methodology yields a more accurate idea about the control of high density microcantilever systems.

To my parents, for their love and support.

ACKNOWLEDGMENTS

I am greatly thankful to my adviser, Professor Petros Voulgaris, for his continuous supervision. His patience and advices have had great contributions to my research work at the Coordinated Science Laboratory (CSL). I am also grateful to Azeem Sarwar and Hussam Sehwail for their support. Finally I would like to express my gratitude appreciation to my parents and my sister for their support and love.

TABLE OF CONTENTS

LIST OF FIGURES

CHAPTER 1

INTRODUCTION

1.1 Microcantilevers in Atomic Force Microscopy

The cantilever is a classical engineering structure whose motion has been heavily studied and is fairly well understood. Put simply, a cantilever is merely a beam that is held rigid at one end. Nanotechnology has led to the creation of microcantilevers. These small scale mechanical structures can be made of materials that can actuate the cantilevers' bending using a voltage. This allows the control and measurement of the beams' microscopic bending and allows for various scientific and industrial applications.

The importance of microcantilevers in the scientific field has been clear since the advent of the atomic force microscope (AFM). While the scanning tunneling microscope was a huge breakthrough, it had serious limitations with regards to observable materials, necessary environments and isolating force effects, which could not be addressed until the invention of the AFM in 1986 by Binnig, Quate, and Gerber [2]. Five years later the AFM was used to show atomic resolution of inert surfaces and there are now thousands of AFMs being used in research labs [2]. The investigation with AFMs includes a wide range of materials from ceramics to biological membranes. Phenomena such as abrasion, adhesion, cleaning, corrosion, etching, friction, lubrication, plating and polishing are studied with this device, gaining great contributions in technologies such as electronics, telecommunications, biotechnology,

materials and computer industries.

The AFM operates by detecting the displacements of a microcantilever tip as the sample surface moves under it. An AFM typically consists of a microcantilever probe, a sample positioner, a detection system for measuring the cantilever deflections and a control system to maintain a desired contact force or a constant distance. A typical setup of an AFM can be seen in Figure 1.1. The AFM has gone through many modifications for specific application requirements and various operational modes evolved over the time. The first one of them is the contact mode, where the tip, being in hard contact with the surface, is deflected as it moves over the surface corrugation. The adjustment of the tip to maintain a constant deflection is displayed as data. Lateral force microscopy is another mode that measures the frictional

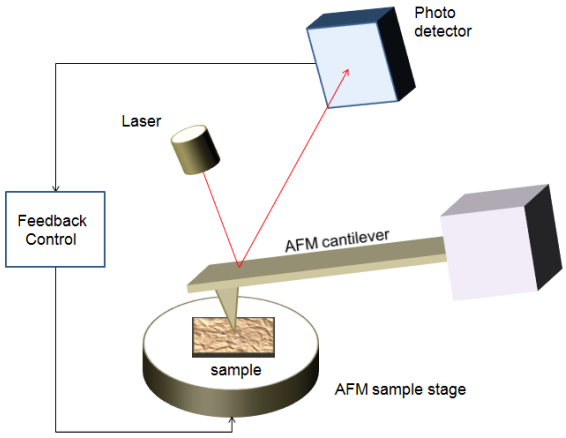

Figure 1.1: Typical AFM Setup

forces on a surface. Noncontact mode is a further technique where the stiff cantilever is oscillated with the tip being quite close to the sample, but not touching it. In this case changes to the resonant frequency or amplitude of the cantilever is measured. Other modes are the tapping mode, where the cantilever operates in a shorter distance than the noncontact mode, having

thus improved lateral resolution; force modulation as a method used to probe properties of materials through sample/tip interactions and finally phase imaging where the phase shift of the oscillating cantilever relative to the driving signal is measured in order to differentiate areas on a sample with such differing areas as friction, adhesion and viscoelasticity.

Microcantilevers have found numerous other applications over the years, having demonstrated success in a variety of sensor applications. They have been able to image and detect biological structures including DNA and proteins [3], [4]. More generally, arrays of piezoelectric microcantilevers can be specially coated and respond to particular substances with the bending response thereby causing a change in voltage resulting in sensitive chemical detectors [5]. Microcantilevers can also be used to detect particular bands of electromagnetic waves, and may serve as more affordable substitutes to current detectors [6]. Additionally, there is the potential for fast, high-density data storage applications, and small scale chips have already been fabricated [7].

1.2 Motivation and Contributions

Electromechanical devices have gone through a significant miniaturization process along with widespread interest in array architectures. Particularly scanning probe devices, AFM being one of them, have thus become versatile instruments with applications ranging from atomic scale multi-probe surface scanning to biosensors. These multi-probe devices are currently designed with large spacing between individual elements in order to eliminate coupling effects. With this practice the individual probes are decoupled and hence can be viewed as isolated objects which significantly simplifies the applications with them. However, at the same time, the throughput of the system is

also reduced. Therefore a revolutionary step in the field of nano-technology calls for the development of a control scheme that can successfully allow independent actuation without compromising the miniaturization and thus the device throughput.

This thesis, leveraging on our previous work in [8] and [9], presents a spatially invariant model of a system of very closely spaced microcantilevers that can be capacitively actuated and sensed independently, and tests it with various controllers. The tests are performed with respect to tracking performance and stability properties. The first one of the controllers is a state feedback, decentralized (meaning each cantilever has its own controller and the controller does not communicate with its neighbors) velocity feedforward controller with a PID component. The second controller is a distributed (meaning each cantilever has its own controller and the controller communicates with the immediate neighbors only), state feedback LQR controller from [22] that is designed with simultaneous localization and optimization. The state feedback controllers are easy to implement, do not involve many calculations and provide quite satisfactory results. Distributed H_∞ controller is the main alternative for the cases where the displacements of the cantilevers are not measurable. In order to obtain a more accurate picture, the control tests are also performed with a more complex, multimodal modeling of the system.

1.3 Organization

Modeling and description of the system is presented in Chapter 2. Chapter 3 introduces 2 types of state feedback controller for the cantilever system; first one being a decentralized feedforward controller with a PID feedback component and second one being a distributed LQR controller, developed from

[22]. In Chapter 4 the formulation of a centralized H_∞ controller for a finite array system is discussed, along with theoretical background on H_∞ control theory. A distributed H_∞ controller and mathematical preliminaries about spatially invariant systems are presented in Chapter 5. Chapter 6 presents a more accurate, multimodal modelling of the same cantilever system using finite element methods (FEM) and results with the previously introduced controllers both in time domain and in frequency domain. Finally, we conclude our discussion in Chapter 7.

CHAPTER 2

SYSTEM MODELING AND DESCRIPTION

2.1 Introduction

The abstract system considered consists of infinitely many microcantilevers connected to the same base and its geometry is shown in Figure 2.1, Figure 2.2 and Figure 2.3. The microcantilevers are capacitively actuated plates with one rigid plate at the bottom and one more flexible plate at the top as shown in Figure 2.1. The top plate is rigid in horizontal direction and can move in vertical direction only. The vertical displacement of each microcantilever is controlled by applying a voltage across the plates. The cantilevers are located in quite close proximity to each other. Therefore, despite each microcantilever's being actuated independently, its dynamics are influenced by the presence of other microcantilevers. As elaborated in Figure 2.2 this influence has two sources: First one is the mechanical coupling because of microcantilevers' being attached to the same base and the second one is the electrical coupling due to the electromagnetic forces applied by the neighboring micro-capacitors. Regarding these the equation of motion for a single cantilever can be written as:

$$\ddot{z}_i + b\dot{z}_i + kz_i = F_{a,i} + F_{mech,i} + F^{\perp}_{elec,i} \tag{2.1}$$

In this equation the subscripts i refer to which cantilever the equation describes. For cantilever i, the symbol z_i is the vertical displacement of the cantilever tip, b is the normalized damping coefficient and k is the concep-

tual spring constant. The spring constant can be rewritten as $k = \omega^2$ with ω being the natural resonant frequency of the i_{th} cantilever.

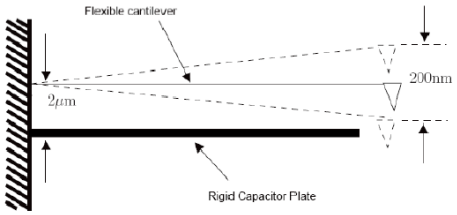

Figure 2.1: A side view of a single cantilever and its respective plate. The cantilever shows a range of vertical motion [8]

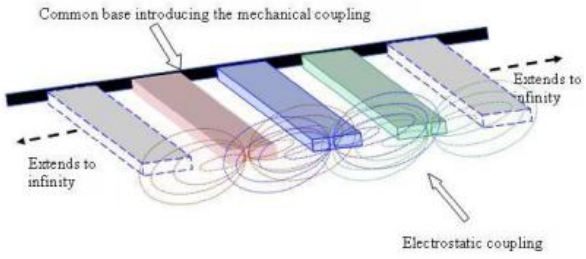

Figure 2.2: Layout of the infinite dimensional microcantilever array with mechanical and electrostatic coupling [8]

$F_{a,i}$ is the force of attraction between the tip of cantilever i and the rigid plate below it. The cantilever's and the rigid plate's acting as electrodes across which voltage is produced cause electrostatic attraction between them having the following formula:

$$F_{a,i} = \frac{\epsilon_0 A}{2md^2}(1 + \frac{2z_i}{d})V_i^2 \tag{2.2}$$

where ϵ_0 is the permittivity of vacuum equal to $8.85 \times 10^{-12} A \cdot s/(V \cdot m)$, A is the area of the cantilever (length by width), d is the gap between the

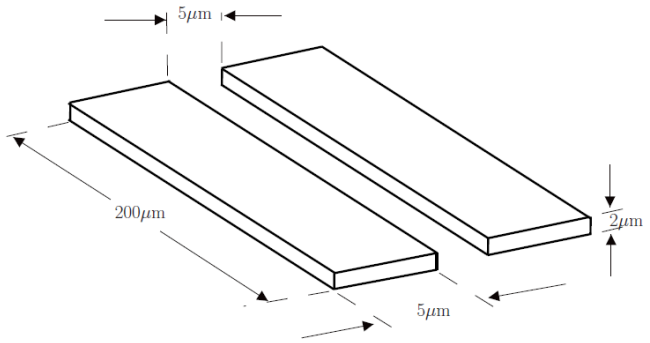

Figure 2.3: Schematic Showing Dimensions of the Cantilevers and Inter-Cantilever Spacing

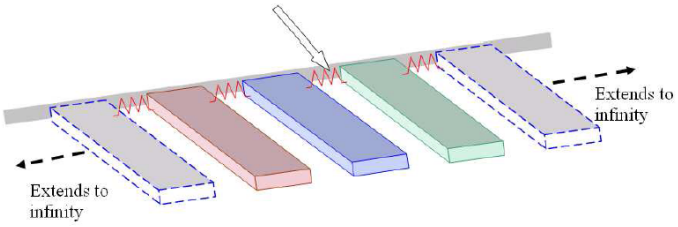

Figure 2.4: Schematic Showing Dimensions of the Infinite Microcantilever Array with Mechanical and Electrostatic Coupling

cantilever and the rigid plate below, m is the mass of the cantilever and V_i is the voltage across the electrodes of cantilever i. The following values for the above parameters were assumed: $d = 2\mu m$; $A = 1 \times 10^{-2}\mu m^2$ [14]. Considering *Cronos polysilicon* [15] to be the material used for the fabrication of microcantilevers, we assume its density as $\rho = 2300kg/m^3$. With the volume of each cantilever taken to be as $v = 2 \times 10^{-14}\mu m^3$. The mass of each cantilever is given as $m = 4.6 \times 10^{-11}kg$.

The mechanical coupling force F_{mech}, exerted on the i_{th} cantilever, can be modeled as follows:

$$F_{mech,i} = \frac{1}{m} \sum_{j=i-1, j\neq i}^{i+1} \gamma_{i,j}(z_j - z_i) \tag{2.3}$$

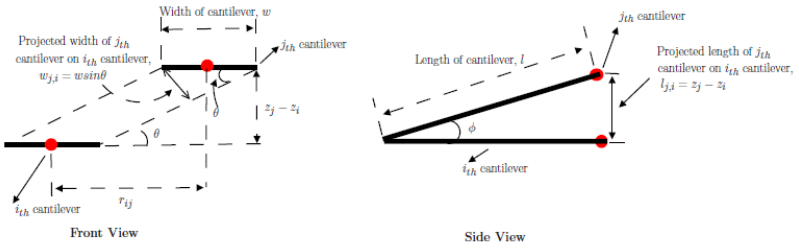

Figure 2.5: Projected Area of j_{th} Cantilever on i_{th} Cantilever

where γ is the mechanical coupling coefficient.The index j refers to the neighboring cantilever.

Finally $F_{elec}^{\perp}$ is the electrostatic coupling between a cantilever and its neighbors:

$$F_{elec}^{\perp} \approx \frac{c_i V_i}{4\pi\epsilon_0} \sum_{j=-\infty, j\neq i}^{\infty} \frac{c_j V_j (z_i - z_j)}{r_{i,j}^3} \tag{2.4}$$

In the next sections the lines introduced in our previous work in [8] and [9] are followed for the modeling of the dynamical system.

2.2 Couplings

2.2.1 Mechanical Coupling

The mechanical coupling can be modeled like a spring force between the bases of the cantilevers, proportional to the difference in the vertical displacement z_i of the cantilevers. Symmetry of the system results in the following properties:

$$\gamma_{i,j} = \gamma_{j,i}, \gamma_{i,j} = \gamma_{i,-j} \tag{2.5}$$

The effect of mechanical coupling is localized in the sense that only the immediate neighbors have a significant mechanical influence on the cantilever. This is also evident in Equation 2.3

2.2.2 Electrostatic Coupling

Using the information from [10], the voltage applied to each capacitor was considered to be including charge on its neighbors, specifically the following expression was considered for the charge on the $i'th$ plate:

$$q_i = c_{i,i}V_{i,i} + \sum_{j=-\infty, j\neq i}^{\infty} c_{i,j}V_{i,j} \tag{2.6}$$

Where

$$c_{i,i} = \epsilon_0 \frac{A}{d - z_i} \tag{2.7}$$

According to the parallel plate capacitor theory the expression of $c_{i,j}$ is given as $c_{i,j} = \epsilon_0 \frac{A_{i,j}}{d_{i,j}}$ where $A_{i,j}$ is the projected area from j_{th} microcantilever to the i_{th} microcantilever and $d_{i,j}$ is the displacement between the centroid of the i_{th} and the j_{th} microcantilever, and z_i, z_j are their respective vertical displacement relative to the mean position, the projected width and length of the j_th cantilever onto i_{th} cantilever can be given as $w_{j,i} = wSin\theta = w\frac{z_j - z_i}{\sqrt{r_{i,j}^2 + (z_i - z_j)^2}}$; $l_{j,i} = z_j - z_i$. Where $w = w_i = w_j$ is width of the i_th cantilever.

The area projected by the j_th cantilever on the i_th cantilever is, thus, given by the following expression

$$A_{j,i} = w_{j,i} \times l_{j,i} = w\frac{(z_j - z_i)^2}{\sqrt{r_{i,j}^2 + (z_i - z_j)^2}} \tag{2.8}$$

The corresponding expression for the capacitance $c_{j,i}$ is therefore given as follows

$$c_{j,i} = \epsilon_0 \frac{w(z_j - z_i)^2}{r_{i,j}^2 + (z_i - z_j)^2} \tag{2.9}$$

In the expression of $c_{j,i}$ in 2.9 it is evident that the charge induced by neighboring cantilevers asymptotes quite rapidly as we move away from the reference cantilever because the rapid decay of $c_{j,i}$ is ensured by the presence

of the term $r_{j,i}^2$ in the denominator. The contribution of charge induced by the neighbors on the reference cantilever is insignificant and hence the expression $\sum_{j=-\infty,j\neq i}^{\infty} c_{i,j}V_{i,j}$ is neglected in the rest of the analysis. Therefore the following expression is used for calculation of charge on the i_th cantilever.

$$q_i = c_{i,i}V_{i,i} \tag{2.10}$$

An electrostatic interaction amongst the microcantilevers occurs due to the charges induced on each microcantilever. As in [10], the interaction between these induced charges is described via a point charge model. Each microcantilever is considered as a charged particle, q_i, and the Coulombs law describes the mutual interaction as follows

$$F_{elec} = \frac{c_i V_i}{4\pi\epsilon_0} \sum_{j=-\infty,j\neq i}^{\infty} \frac{c_j V_j}{r_{i,j}^2} \tag{2.11}$$

and the vertical component of this force is given as

$$F_{elec}^{\perp} = \frac{c_i V_i}{4\pi\epsilon_0} \sum_{j=-\infty,j\neq i}^{\infty} \frac{c_j V_j (z_i - z_j)}{r_{i,j}^2\sqrt{r_{i,j}^2 + (z_i - z_j)^2}} \approx \frac{c_i V_i}{4\pi\epsilon_0} \sum_{j=-\infty,j\neq i}^{\infty} \frac{c_j V_j (z_i - z_j)}{r_{i,j}^3} \tag{2.12}$$

2.3 Linearization

The lineariztation of the nonlinear system given in 2.1 around some equilibrium point is necessary in order to apply frequency domain stability and robustness analysis. The states of the system are $x_{i,1}{:=}z_i$ for the displacement of the cantilever, $x_{i,2}{:=}\dot{z}_i$ for the velocity of the cantilever, $x_{i,3}{:=}V_i$ for the applied voltage on the cantilever. The state equations are formed as follows:

$$\begin{aligned} \dot{x}_{i,1} &= x_{i,2} \\ \dot{x}_{i,2} &= -bx_{i,2} - \omega^2 x_{i,1} + F_{a,i} + F_{mech,i} + F_{elec,i}^{\perp} \end{aligned} \tag{2.13}$$

In the operation of an AFM, the microcantilevers are required to operate away from their zero displacement position. Therefore an initial DC offset for all the microcantilevers is assumed as the starting point. The equilibrium position is thus calculated as follows. Assuming $V_i = V_j = V_e$ and $x_{ei} = x_{ej} = x_e$

$$\begin{aligned}
\dot{x}_{e1} &= x_{e2} = 0 \\
\dot{x}_{e2} &= -bx_{e2} - \omega^2 x_{e1} + F^e_{a,i} + F^e_{mech,i} + F^{e\perp}_{elec,i} = 0 \\
&\Rightarrow -\omega^2 x_{e1} + F^e_{a,i} + F^e_{mech,i} + F^{e\perp}_{elec,i} = 0
\end{aligned} \tag{2.14}$$

Where

$$\begin{aligned}
F^e_{a,i} &= \frac{\epsilon_0 A}{2md^2}(1 + \frac{2x_{e1}}{d})V_e^2 \\
F^e_{mech,i} &= \frac{1}{m}\sum_{j=i-1, j\neq i}^{i+1} \gamma_{i,j}(x_{e1j} - x_{e1i}) = 0; (x_{e1i} = x_{e1j}) \\
F^{e\perp}_{elec} &= \frac{c_i V_i}{m4\pi\epsilon_0}\sum_{j=-\infty, j\neq i}^{\infty} \frac{c_j V_j (x_{e1i} - x_{e1j})}{r^3_{i,j}} = 0; (x_{e1i} = x_{e1j})
\end{aligned}$$

Thus we have

$$\begin{aligned}
\omega^2 x_{e1} &= \frac{\epsilon_0 A}{2md^2}(1 + \frac{2x_{e1}}{d})V_e^2 \\
\frac{\epsilon_0 A}{2}V_e^2 &= x_{e1}(\frac{\omega^2 md^3 - \epsilon_0 A V_e^2}{d}) \\
x_{e1} &= \frac{\epsilon_0 A V_e^2 d}{2(\omega^2 md^3 - \epsilon_0 A V_e^2)}
\end{aligned}$$

The first order approximation for the expression of capacitance for the i_{th} cantilever can be given as follows:

$$c_i = \epsilon_0 \frac{A}{d - z} = \epsilon_0 \frac{A}{d} \cdot \frac{1}{d(1 - \frac{z}{d})} = \epsilon_0 \frac{A}{d}\left(1 + \frac{z}{d} + \frac{z^2}{d^2} + \ldots\right) \tag{2.15}$$

Where we used the fact that $d > z$. Neglecting the higher order terms we get

$$c_i = \epsilon_0 \frac{A}{d}\left(1 + \frac{z}{d}\right) \tag{2.16}$$

Now the linearization of $F_{a,i}$ yields

$$\begin{aligned}\tilde{F}_{a,i} &= \frac{\epsilon_0 A}{md^2} V_e \cdot V_i + \frac{\epsilon_0 A V_e^2}{md^3} \cdot x_{i,1} + \frac{2\epsilon_0 A x_{e1} V_e}{md^3} \cdot V_i \\ &= (\frac{\epsilon_0 dA V_e + 2\epsilon_0 A x_{e1} V_e}{md^3}) V_i + \frac{\epsilon_0 A V_e^2}{md^3} x_{i,1} \end{aligned} \tag{2.17}$$

Similarly, given the following expression of $F^{\perp}_{elec,i}$

$$F^{\perp}_{elec,i} = \epsilon_0 \frac{A}{d}\left(1+\frac{z}{d}\right)\frac{V_i}{m4\pi\epsilon_0}\sum_{j=-\infty, j\neq i}^{\infty} \epsilon_0 \frac{A}{d}\left(1+\frac{z_j}{d}\right)\frac{V_j(z-z_j)}{r_{i,j}^3} \tag{2.18}$$

we can derive the expression for its linearization. With the calculations introduced in [9] we get the linearized equation for $F^{\perp}_{elec,i}$ in the state space notation as follows

$$F^{\perp}_{elec,i} = (1+\frac{x_{e1}^2}{d^2}+\frac{2x_{e1}}{d})\epsilon_0 \frac{A^2 V_e^2}{4md^2\pi}\sum_{j=-\infty, j\neq i}^{\infty}\frac{(x_{i,1}-x_{j,1})}{r_{i,j}^3} \tag{2.19}$$

The linearized equations of motion for the i_{th} cantilever can be written as

$$\begin{aligned}\dot{x}_{i,1} &= x_{i,2} \\ \dot{x}_{i,2} &= -bx_{i,2} - x_{i,1}\left(\omega^2 - \frac{\epsilon_0 A V_e^2}{md^3}\right) \\ &+ \left(\frac{\epsilon_0 dA V_e + 2\epsilon_0 A x_{e1} V_e}{md^3}\right) V_i + \frac{1}{m}\sum_{j=i-1, j\neq i}^{i+1}\gamma_{i,j}(\delta x_{1ji}) \\ &- \left(1+\frac{x_{e1}^2}{d^2}+\frac{2x_{e1}}{d}\right)\epsilon_0\frac{A^2V_e^2}{4md^2\pi}\sum_{j=-\infty, j\neq i}^{\infty}\frac{\delta x_{1ji}}{r_{i,j}^3} \\ \dot{x}_{i,3} &= u_i \end{aligned} \tag{2.20}$$

with u_i being the input to the i_{th} cantilever and $\delta x_{1ji} = x_{j,1} - x_{i,1}$. The current generated as a result of the excitation of microcantilevers is considered as the output of the system and its expression is given as

$$y = \frac{\mathrm{d}(c_i V_i)}{\mathrm{dt}} \tag{2.21}$$

Where

$$c_i = \frac{\epsilon_0 A}{(d-z)} = \frac{\epsilon_0 A}{d(1-\frac{d}{z})} = \frac{\epsilon_0 A}{d}\cdot\frac{1}{(1-\frac{d}{z})} \tag{2.22}$$

since $d > z$

$$c_i = \frac{\epsilon_0 A}{d}(1 + \frac{z}{d} + \left(\frac{z}{d}\right)^2 + \left(\frac{z}{d}\right)^3 + \ldots) \tag{2.23}$$

the first order approximation is given as

$$c_i = \frac{\epsilon_0 A}{d}(1 + \frac{z}{d}) \Rightarrow \frac{\mathrm{d}(c_i)}{\mathrm{dt}} = \frac{\epsilon_0 A}{d^2}\dot{z} \tag{2.24}$$

We have

$$y_i = \mathrm{d}\frac{c_i V_i}{\mathrm{dt}} = \frac{V_i \epsilon_0 A}{d^2}\dot{x}_{i,1} + \frac{\epsilon_0 A}{d}\dot{V}_i + \frac{\epsilon_0 A x_{i,1}}{d^2}\dot{V}_i \tag{2.25}$$

This equation of output can be linearized as below:

$$y_i = \frac{V_e \epsilon_0 A}{d^2}x_{i,2} + \dot{V}_i\left(\frac{\epsilon_0 A}{d} + \frac{\epsilon_0 A x_{e1}}{d^2}\right) \tag{2.26}$$

2.4 Spatio-Temporal Scaling

The dynamics of the system need to be scaled in terms of amplitude and time in order to improve the computational efficiency. In doing so we define

$\hat{x} = \delta_x x$, where $\delta_x = 10^6$, and we measure $\hat{x}$ in micro meters

$\hat{y} = \delta_y y$, where $\delta_y = 10^6$, and we measure $\hat{y}$ in micro amperes

$\hat{V}_i = \delta_V V_i$, where $\delta_V = 10^3$, and we measure $\hat{V}_i$ in milli volts

$\tau = \omega_0 t$, where $\omega_0 = 10^3$, and we measure τ in milliseconds. The corresponding equilibrium point $\hat{x}_{e1}$ is given as

$$\hat{x}_{e1} = \frac{\epsilon_0 A \hat{V}_e^2 d\delta_x}{2(\omega^2 m d^3 \delta_x - \epsilon_0 A \hat{V}_e^2)} \tag{2.27}$$

The scaled equations of motion for the i_{th} cantilever hence can be given as follows

$$\dot{\hat{x}}_{i,1} = \frac{1}{\omega_0}\hat{x}_{i,2}$$

$$\dot{\hat{x}}_{i,2} = -\frac{b}{\omega_0}\hat{x}_{i,2} - \hat{x}_{i,1}\frac{1}{\omega_0^2}\left(\omega^2 - \frac{\epsilon_0 A V_e^2}{md^3\delta_V^2}\right)$$
$$+ \left(\frac{\epsilon_0 A\hat{V}_e}{md^2\omega_0^2} + \frac{2\epsilon_0 A\hat{x}_{e1}\hat{V}_e}{md^3\omega_0^2\delta_V^2}\right)\frac{\delta_x}{\delta_V}\hat{V}_i + \frac{1}{m\omega_0^2}\sum_{j=i-1,j\neq i}^{i+1}\gamma_{i,j}(\delta\hat{x}_{1ji})$$
$$- \left(1 + \frac{\hat{x}_{e1}^2}{d^2\delta_x^2} + \frac{2\hat{x}_{e1}}{d\delta_x}\right)\epsilon_0\frac{A^2\hat{V}_e^2}{4md^2\pi\omega_0^2\delta_V^2}\sum_{j=-\infty,j\neq i}^{\infty}\frac{\delta\hat{x}_{1ji}}{r_{i,j}^3}$$

The expression for the output of the system is similarly given as follows

$$\hat{y}_i = \frac{V_e\epsilon_0 A}{d^2}\hat{x}_{i,2} + \dot{\hat{V}}_i\frac{\delta_x}{\delta_V}\omega_0\left(\frac{\epsilon_0 A}{d} + \frac{\epsilon_0 A\hat{x}_{e1}}{d^2}\right) \tag{2.28}$$

Define the following

$$\tilde{A} = \begin{bmatrix} 0 & \frac{1}{\omega_0} & 0 \\ a_{21} & -\frac{b}{\omega_0} & a_{23} \\ 0 & 0 & 0 \end{bmatrix} \tag{2.29}$$

where

$$a_{21} = -\frac{\omega^2}{\omega_0} + \frac{\epsilon_0 A\hat{V}_e^2}{\omega_0^2 md^3\delta_V^2} + \left(1 + \frac{\hat{x}_{e1}^2}{d^2\delta_x^2} + \frac{2\hat{x}_{e1}}{d\delta_x}\right)\epsilon_0\frac{A^2\hat{V}_e^2}{d^2 m4\pi\omega_0^2\delta_V^2}\sum_{j=-\infty,j\neq i}^{\infty}\frac{1}{r_{i,j}^3}$$
$$- \frac{1}{m\omega_0^2}\sum_{j=i-1,j\neq i}^{i+1}\gamma_{i,j} \tag{2.30}$$

$$a_{23} = \frac{\delta_x}{\delta_V}\left(\frac{2\hat{x}_{e1}\epsilon_0 A\hat{V}_e}{md^3\omega_0^2\delta_V^2} + \frac{\epsilon_0 A\hat{V}_e}{md^2\omega_0^2}\right) \tag{2.31}$$

The B matrix is

$$\hat{B} = \begin{bmatrix} 0 \\ 0 \\ 1 \end{bmatrix} \tag{2.32}$$

For the coupling from the neighbors

$$\hat{G}_{i,j} = \sum_{j=-\infty,j\neq i}^{\infty}\begin{bmatrix} 0 & 0 & 0 \\ \frac{1}{m\omega_0^2}\gamma_{i,j} - \left(1 + \frac{\hat{x}_{e1}^2}{d^2\delta_x^2} + \frac{2\hat{x}_{e1}}{d\delta_x}\right)\epsilon_0\frac{A^2\hat{V}_e^2}{d^2 m4\pi\omega_0^2\delta_V^2}\frac{1}{r_{i,j}^3} & 0 & 0 \\ 0 & 0 & 0 \end{bmatrix} \tag{2.33}$$

Where the fact that $\gamma_{i,i+k} = 0$ for $\|k\| > 1$ is used. Finally the output matrix and feedthrough matrix are written as:

$$\hat{C} = \begin{bmatrix} 0 & \frac{\hat{V}_e \epsilon_0 A}{d^2} & 0 \end{bmatrix}; \hat{D} = \left[\frac{\delta_x}{\delta_V} \omega_0 \left(\frac{\epsilon_0 A}{d} + \frac{\epsilon_0 A \hat{x}_{e1}(t)}{d^2} \right) \right] \tag{2.34}$$

The above equations are derived for the i_{th} cantilever which has the following states:

$$\hat{x}_i = \begin{bmatrix} \hat{x}_1 \\ \hat{x}_2 \\ \hat{x}_3 \end{bmatrix} \tag{2.35}$$

and the following state space formulation:

$$\dot{\hat{x}}_i = \tilde{A}\hat{x}_i + \sum_{j=-\infty, j\neq i}^{\infty} \hat{G}_{i-j}\hat{x}_j + \tilde{B}\dot{\hat{V}}_i \tag{2.36}$$

$$\hat{y}_i = \tilde{C}\hat{x}_i + \tilde{D}\dot{\hat{V}}_i \tag{2.37}$$

The entire system however has infinitely many cantilevers with the following global state variable:

$$\eta = \begin{bmatrix} \vdots \\ \hat{x}_{-1} \\ \hat{x}_0 \\ \hat{x}_1 \\ \vdots \end{bmatrix} \tag{2.38}$$

and the following state space formulation:

$$\dot{\eta} = \begin{bmatrix} & \ddots & \dots & & & & \\ \dots & \hat{G}_{-1} & \tilde{A} & \hat{G}_1 & \hat{G}_2 & & \\ \dots & \hat{G}_{-2} & \hat{G}_{-1} & \tilde{A} & \hat{G}_1 & \hat{G}_2 & \dots \\ & \dots & \hat{G}_{-2} & \hat{G}_{-1} & \tilde{A} & \hat{G}_1 & \dots \\ & & & \vdots & \ddots & \ddots & \end{bmatrix} \eta + \begin{bmatrix} \vdots \\ \tilde{B}u_{-1} \\ \tilde{B}u_0 \\ \tilde{B}u_1 \\ \vdots \end{bmatrix} \tag{2.39}$$

2.5 Modes

We note that in our preceding discussion of modelling the cantilever arrays we have focused on a simple model with only a single mode. This is just an approximation that makes the design simpler. In order to make the results more accurate we may wish to consider multiple modes. Finite element method (FEM) is a potential method for this where one can divide the beam into several smaller, interconnected beam elements. The equations describing the interaction of the beam elements give the rate of change of the points between elements. The results are fed into a numerical differential equation solver in iterations until a particular amount of time has been solved for. This method has been shown to be fairly accurate in describing beams [13] and is going to be explained further in chapter 6. The chapters 3, 4, 5 are about the control design on the simple, single mode model.

CHAPTER 3

STATE FEEDBACK CONTROL

3.1 Introduction

In this section two sorts of state feedback controllers are introduced to the cantilever system. The first one is a PID plus feedforward controller where each cantilever has its own local controller and each controller is fully decentralized, i.e. it only uses the information from its own cantilever. The gains of the PID controller and the feedforward gain are adjusted for the best performance. The second one is a structured optimal state feedback controller introduced in [22]. This controller is constructed using augmented Lagrangian method. Each cantilever has its own controller that are not fully decentralized but use only immediate neighbor information. It should be noted that both controllers use state information of the cantilevers and thus they would represent a benchmark for simple controller systems if the states are measurable.

3.2 Feedforward Controller with State Feedback

The PID control is the most common form of feedback control and is quite useful in setpoint tracking. In addition to this it is easy to implement. However, a simple PID controller may not provide enough tracking performance especially if the reference is time varying. In this case a coupling from the input signal, which can be the reference or a disturbance, is directly added to

the control variable. Requiring the knowledge of system parameters and reference, this combined feedforward-feedback control can significantly improve tracking performance for time-varying reference with even high frequencies.

3.2.1 Controller Design

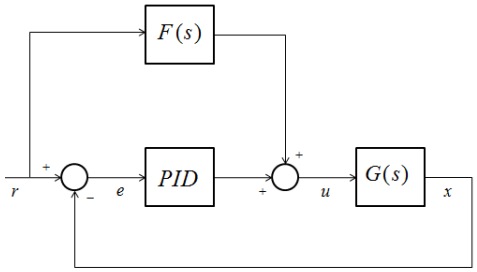

Figure 3.1: Block Diagram for the Feedforward Controller

As shown in Figure 3.1 the feedforward component comes from the reference. $G(s)$ is the plant transfer function and $F(s)$ is the feedforward function. The error is a vector of differences between the displacement of the cantilevers and the reference vector. For a single cantilever the PID controller has the following formula:

$$u_{i,PID} = k_p \cdot e_i + k_d \cdot \dot{e}_i + k_i \cdot \int e_i \tag{3.1}$$

$$e_i = r_i - \hat{x}_{i,1} \tag{3.2}$$

with k_p, k_d, k_i, e_i being the proportional gain, derivative gain, integral gain and the tracking error for the i_{th} cantilever respectively.

In many cases the feedforward component $F(s)$ is chosen to be the inverse of the plant transfer function $G(s)$. This makes the reference to state transfer function $(G \cdot F + G \cdot PID)/(I + G \cdot PID)$ equal to 1, meaning perfect tracking. This choice for $F(s)$ is however not always feasible because of the

non-minimum phase behavior of the plant. In addition to this, the cantilever model presented in this paper has nonlinearities and coupling effects from its neighbors which makes it harder to have an inverted transfer function of the single cantilever. Therefore, for the nonlinear cantilever array system velocity feedforward control is used with the feedforward component being the derivative of the reference scaled with a constant gain:

$$u_{i,F} = k_f \cdot \dot{r_i} \tag{3.3}$$

So the whole system's controller can be written as:

$$u = (k_p \cdot e_i + k_d \cdot \dot{e_i} + k_i \cdot \int e_i + k_f \cdot \dot{r_i}) \cdot I \tag{3.4}$$

with I being the $n \times n$ identity matrix, where n is the number of cantilevers. The whole system's controller can be designed in such way since the individual controllers do not use any neighbor information. By choosing appropriate values for the controller gains one can achieve quite satisfactory results.

3.2.2 Simulation of the Nonlinear System

Simulations are done with a 21 cantilever-nonlinear system having the decentralized feedforward control. The reference input has a frequency of 3000 rad/sec with an amplitude of 10 nm for each cantilever. The tracking errors of 5 cantilevers in the array are shown in Figure 3.2. The cantilevers have all tracking errors less than 1 nm. Also the reference input along with the tracked output for two sample cantilevers is presented in Figure 3.3.

Despite the good tracking results at a frequency of 3000 rad/sec for all the cantilevers the tracking performance deteriorates as the frequency is varied along the cantilever array. Figure 3.4 shows the absolute tracking error of 8 cantilevers having different excitation frequencies. Although the maximum frequency is 3000 rad/sec some cantilevers have unacceptable tracking errors

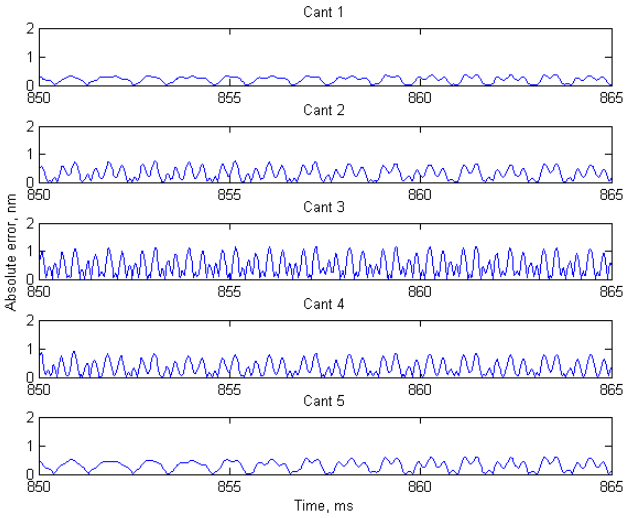

Figure 3.2: Feedforward Control design: Tracking error of 5 cantilevers in a system of 21 cantilevers. In all the above cases the excitation frequency and amplitude are 3000rad/sec and 10nm respectively

as high as 10 nm. The comparison of the reference input and the tracked output for 2 cantilevers, and thus the deterioration of the tracking performance, can be seen in Figure 3.5.

Using standard tuning techniques control effort has to be kept below certain limits. The control effort in this design was always below $\pm 7V$ as shown in Figure 3.9.

3.2.3 Stability and Robustness Analysis

The previous sections show that the feedforward controller yields satisfactory results with tracking errors within acceptable limits, up to a reference frequency of 3000 rad/sec. The sensitivity analysis is an important tool to further determine performance and robustness characteristics of the design. The bandwidth of the Bode plot of reference to error transfer function is a good indicator for this. In order to have the full information of the cantilever

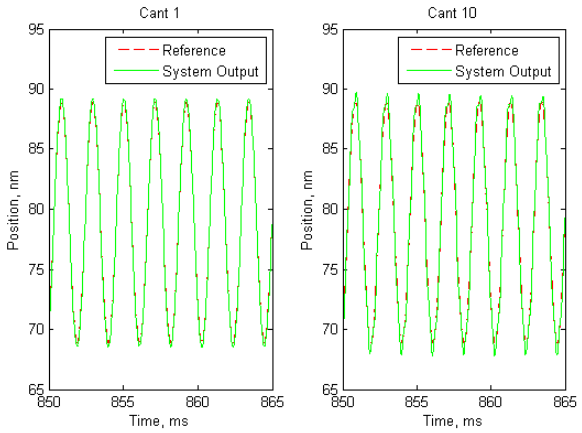

Figure 3.3: Feedforward Control design: Reference input and tracked output for two sample cantilevers. In all the above cases the excitation frequency and amplitude are 3000rad/sec and 10nm respectively

system the singular value plots are drawn in Figure 3.10 in an array of 5 cantilevers. The feedforward controller has a bandwidth of between 12000-14000 rad/sec.

A similar analysis can be done with the Linear Spatial Time Invariant (LSTI) infinite abstraction that is explained as follows. The A matrix of a single cantilever in an array of infinitely many cantilevers can be written as:

$$\begin{aligned} A = ... + A_{-2}S^{-2} + A_{-1}S^{-1} + A_0 \\ + A_1S^1 + A_2S^2... \end{aligned} \tag{3.5}$$

with S as the spatial shift operator associated with coupling from neighbors. A good LSTI model can be obtained by using only a 2 neighbor interaction. In this case the A matrix in a spatial Fourier transform representation would be:

$$\begin{aligned} A(\theta) = A_{-2}e^{-2j\theta} + A_{-1}e^{-j\theta} + A_0 \\ + A_1e^{j\theta} + A_2e^{2j\theta} \end{aligned} \tag{3.6}$$

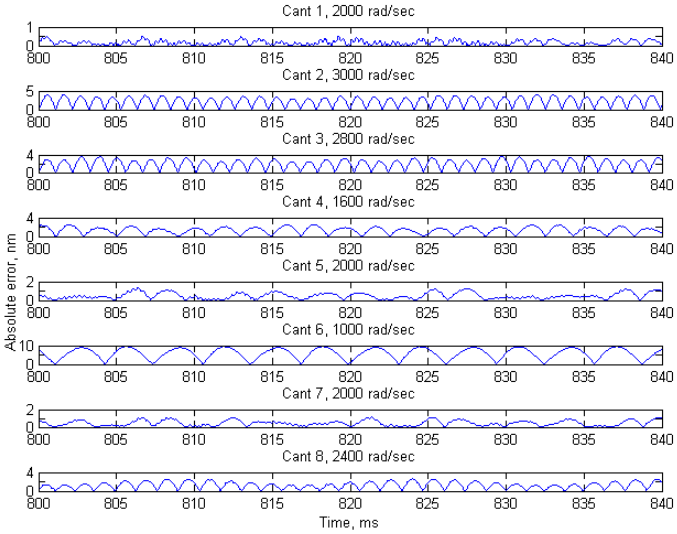

Figure 3.4: Feedforward Control design: Absolute Tracking error of 8 cantilevers in an array of 21 cantilevers at different excitation frequencies

with θ being the spatial frequency over $[0\ 2\pi]$. Figure 3.11 shows the resulting reference to error Bode plot for the feedforward controller, using various values of the spatial frequency θ. The result is very similar to the singular value plot in Figure 3.10. So a finite system with a high number of cantilevers is not expected to lead to any different analysis. The numerical experiments show that at a frequency of 4500 rad/sec the maximum absolute tracking error is 1.5nm. However, at frequencies higher than 5000 rad/sec the feedforward controller can be unstable. Instability is always the case for this controller at frequencies higher than 12000 rad/sec.

A traditional way of analyzing the stability robustness of a system is calculating its phase and gain margins. Phase margin is the amount of additional phase lag at the gain crossover frequency required to make the system unstable and gain margin is the additional loop gain causing instability. For a stability analysis both of them have to be calculated. The feedforward con-

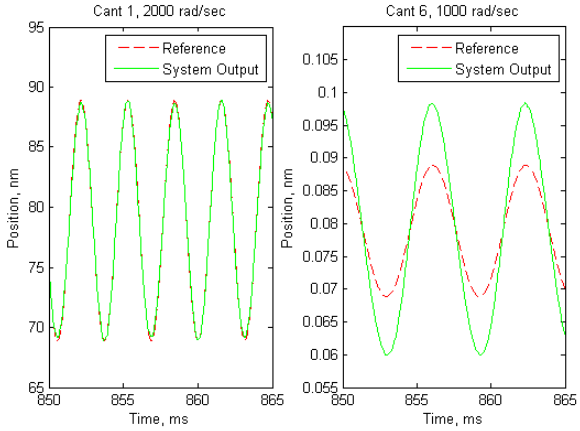

Figure 3.5: Feedforward Control design: Reference input and tracked output of two sample cantilevers in a system of 21 cantilevers at different excitation frequency

trol system's open loop transfer function has a phase margin of 9.53 degrees and its gain margin is 7.25 dB, as shown in Figure 3.12. The closed loop system is stable since both of the values are positive and the gain margin is above 6 dB which is usually desired. However the phase margin is low which means that a phase shift or change of some parameters may result in instability. According to simulations instability is not the case at frequencies as high as 3000 rad/sec however beyond this frequency phase shifts can yield undesired results. Note that these results are also compatible with the high peak value of the reference to error Bode plot of the feedforward controller in Figure 3.10 and Figure 3.11 since the high H_∞ norm of the sensitivity function indicates poor robustness of the system. The actual system may have some uncertainties at its parameters. In order to have a better idea about the actual system behavior robustness analysis is performed.

$$\hat{M}(s,\lambda) := F_l(\hat{G}(s,\lambda), \hat{K}(s,\lambda)) \tag{3.7}$$

Where s and λ represent laplace and fourier transform variables for the tem-

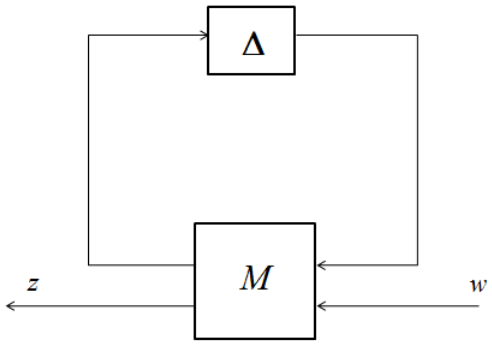

Figure 3.6: General Setup for Robust Stability

poral and spatial frequencies respectively. The perturbation δ to the nominal model is defined as to be having the following usual block diagonal structure;

$$\mathbf{\Delta} = \{diag[\delta_1 I_{r1}, \ldots, \delta_s I_{rs}, \Delta_1, \ldots, \Delta_F]\} \ : \ \delta_i \in \mathcal{C}, \Delta_j \in \mathcal{C}^{m_j \times m_j} \tag{3.8}$$

The structured singular value $\mu_\Delta(M(s,\lambda))$ which is an important tool for robustness analysis is defined as follows

Definition 1. *$\mu_\Delta(M(s,\lambda))$ is defined as*

$$\mu_\Delta(M(s,\lambda)) := \frac{1}{min\{\bar{\sigma}(\Delta) : det(I - M(s,\lambda)\Delta) = 0, \Delta \in \mathbf{\Delta}\}} \tag{3.9}$$

where $\mathbf{\Delta}$ is as defined above and $\bar{\sigma}(\Delta)$ is the largest singular value (operator norm) of the block matrix Δ.

So literally, if one finds the smallest structured perturbation Δ (measured in terms of its maximum singular value $\bar{\sigma}(\Delta)$) that brings the system to the verge of instability then $\frac{1}{\mu}$ is the magnitude of this perturbation, meaning its maximum singular value. A relatively large μ means that a small perturbation can make the system unstable, resulting in relatively bad robust stability.

Based on the small gain theorem, the robust stability theorem for systems with structured uncertainties is then the following:

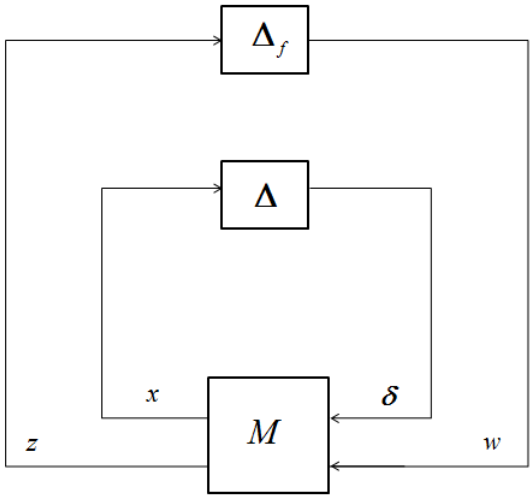

Figure 3.7: Setup for Robust Performance with Ficticious Δ_f

Theorem 1. *Let $\beta > 0$. For all $\Delta \in \mathcal{D}(\mathbf{\Delta})$ with $\|\Delta\|_\infty < \frac{1}{\beta}$ the loop shown in Figure 3.6 is well-posed, internally stable, and $\|\mathcal{F}(M_p(j\omega, e^{j\theta}), \Delta)\|_\infty \leq \beta$ if and only if*

$$\sup_{\omega \in \mathcal{R}, \theta \in [0, 2pi]} \mu_{\mathbf{\Delta}_P}(M_p(j\omega, e^{j\theta})) \leq \beta \tag{3.10}$$

Where $\mathcal{D}$ denote the set of all block diagonal and stable rational transfer functions that have the block structure such as $\mathbf{\Delta}$.

$$\mathcal{D}(\mathbf{\Delta}) = \{\Delta(\cdot) \in RH_\infty : \Delta(s_o) \in \mathbf{\Delta} \forall s_o \in \bar{\mathcal{C}}_+\} \tag{3.11}$$

This theorem is also useful for the analysis of the robust tracking performance of the system. The robust performance problem can be converted in to a robust stability problem by adding a fictitious block Δ_f between the error as the closed loop system output(z) and the tracking reference as the external input to the closed loop system (w); depicted in 3.7. The augmented block structure of the perturbation is then defined as follows

$$\mathbf{\Delta}_p = \begin{bmatrix} \Delta & 0 \\ 0 & \Delta_f \end{bmatrix} : \Delta \in \mathbf{\Delta}, \Delta_f \in \mathcal{C}^{q_2 \times p_2} \tag{3.12}$$

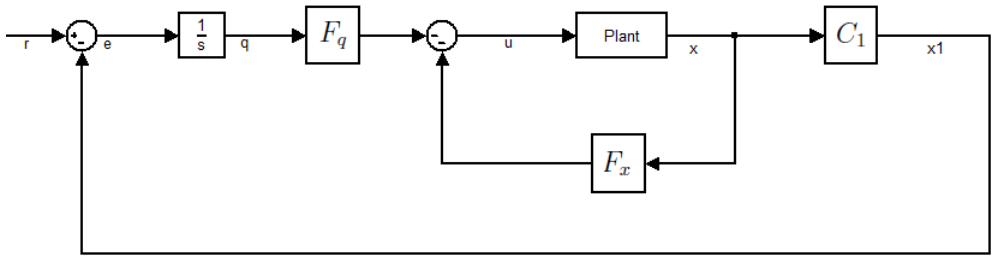

Figure 3.8: Setup for LQR Control with Integral Augmentation

The μ analysis is then performed on the closed loop system with this uncertainty structure.

In equations 2.30 and 2.31 a_{21} and a_{23} are defined and $a_{22} = -\frac{b}{\omega_0}$. For the robustness analysis of the finite system an array of 5 cantilevers is considered and the perturbations are introduced in the following way:

$$\begin{aligned} \overline{a_{21}} &= a_{21} + \delta_1 \\ \overline{a_{22}} &= a_{22} + \delta_2 \\ \overline{a_{23}} &= a_{23} + \delta_3 \end{aligned} \tag{3.13}$$

where $\delta_i \in \mathbb{C}$ is the size of uncertainty. The plot of the structured singular value for the system having the above uncertainty structure and consisting of 5 cantilevers can be seen in Figure 3.13. The plot has a quite high peak at frequencies close to 20000 rad/sec.

For the infinite abstraction $a_{21}(\theta)$ is defined:

$$\begin{aligned} a_{21}(\theta) = &- \frac{\omega^2}{\omega_0} + \frac{\epsilon_0 A \hat{V}_e^2}{\omega_0^2 m d^3 \delta_V^2} - \left(1 + \frac{\hat{x}_{e1}^2}{d^2\delta_x^2} + \frac{2\hat{x}_{e1}}{d\delta_x}\right) \epsilon_0 \frac{A^2 \hat{V}_e^2}{d^2 m 4\pi\omega_0^2 \delta_V^2} \sum_{l=-\infty, l\neq k}^{\infty} \frac{1}{r_{k,l}^3}(e^{jl\theta} - 1) \\ &+ \frac{1}{m\omega_0^2} \sum_{l=k-1, l\neq k}^{k+1} \gamma_{k,l}(e^{jl\theta} - 1) \end{aligned} \tag{3.14}$$

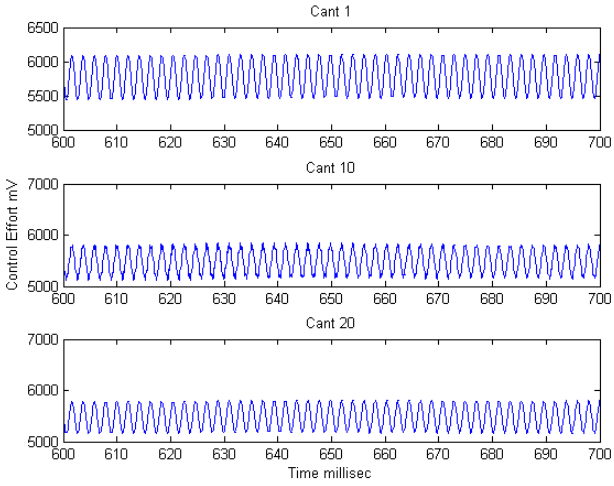

Figure 3.9: Feedforward Control design: Control Effort of 6 cantilevers in a 21 cantilever system. In all the above cases the excitation frequency and amplitude are 3000rad/sec and 10nm respectively

with θ being the spatial frequency. The perturbations are defined

$$\begin{aligned} \overline{a_{21}(\theta)} &= a_{21}(\theta) + \delta_1(\theta) \\ \overline{a_{22}} &= a_{22} + \delta_2 \\ \overline{a_{23}} &= a_{23} + \delta_3 \end{aligned} \tag{3.15}$$

The plot of the structured singular value for the system that is modeled with the infinite abstraction and that has the above uncertainty structure can be seen in Figure 3.14. Similar to the finite model the structured singular value has high magnitudes especially at frequencies close to 20000 rad/sec. In the next sections the structured singular value analysis is done for the optimal state feedback controller from [22] that has significantly lower structured singular value for the same uncertainty structure, meaning better robustness properties.

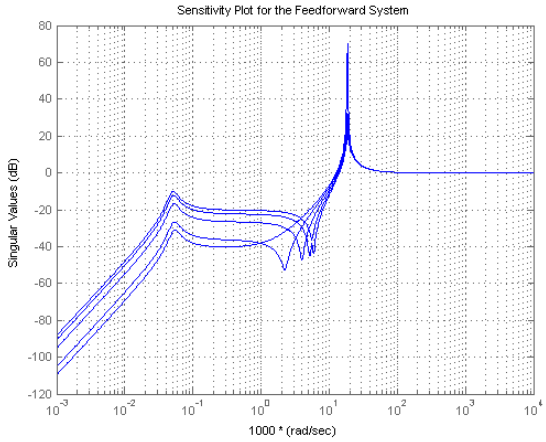

Figure 3.10: Sensitivity Plot of the Feedforward Control System for an array of 5 cantilevers

3.3 Optimal State Feedback Controller

In this section the controller introduced in [22] is implemented in the cantilever system. The optimal state feedback control is obtained in such a way that both the cost function, which is the tracking error in this case, and the neighbor information are minimized simultaneously. The minimizer of this constrained optimal control problem is sought using the augmented Lagrangian method.

3.3.1 Problem Formulation and Augmented Lagrangian Method

Let a linear time-invariant system be given by its state space representation

$$\begin{aligned} \dot{x} &= Ax + B_1 d + B_2 u \\ z &= \begin{bmatrix} Q^{1/2} \\ 0 \end{bmatrix} x + \begin{bmatrix} 0 \\ R^{1/2} \end{bmatrix} u \end{aligned} \tag{3.16}$$

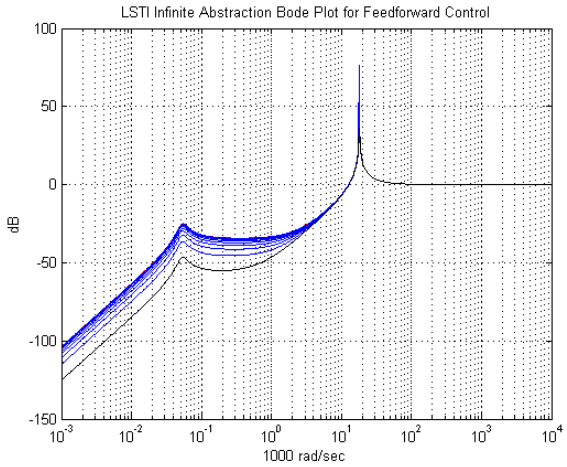

Figure 3.11: LSTI infinite abstraction bode magnitude plot of reference to error transfer function for one cantilever using Feedforward Control (red for $\theta = 0$, black for $\theta = 2\pi$, magnitude in dB, frequency in $10^3 rad/sec$)

where x is the state vector, d is the disturbance, u is the control input and z is the performance output. $Q^{1/2}$ and $R^{1/2}$ denote the square roots of the state and control performance weights. The structured state feedback design problem is considered

$$u = -Fx \tag{3.17}$$

where matrix F has to satisfy some structural constraints. Let the subspace $\mathcal{S}$ symbolize these structural constraints and let us assume that there exists a non-empty set of stabilizing F that belongs to $\mathcal{S}$. The objective is to design a control $F \in \mathcal{S}$ that minimizes H_2 norm of the transfer function from d to z. This structured optimal control problem can be formulated as an LQR type cost function $J(F)$ subject to the constraint that $F \in \mathcal{S}$. $\mathcal{S}$ in this work represents the set of diagonal matrices with the minimum number of zeros. Hence the objective is minimizing the cost function (the H_2 norm of the reference to error transfer function) and diagonalizing F by minimizing

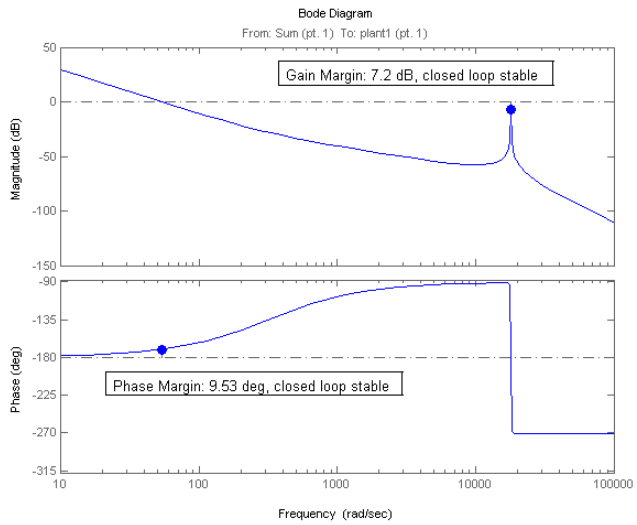

Figure 3.12: Phase and gain margins of the Feedforward Control System for an isolated cantilever

the number of zeros simultaneously, as indicated below:

$$\text{minimize} \quad J(F) + \gamma card(F) \tag{3.18}$$

The cardinality function $card(F)$ represents the number of nonzero elements of F. Mathematically this corresponds to a function having the value 0 for $|F_{ij}| = 0$ and a nonzero constant value (for instance 1) otherwise. γ is a non-negative number indicating the importance of sparsity of F. The higher the value of γ the more decentralized the controller becomes. The equation 3.18 represents a strike balance between the sparsity of F and the variance amplification from d to z and this is depicted by two functions J and g. In order to decouple these functions the problem is defined in the following way:

$$\text{minimize} \quad J(F) + \gamma g(\hat{F}) \tag{3.19}$$

$$\text{subject to} \quad F - \hat{F} = 0 \tag{3.20}$$

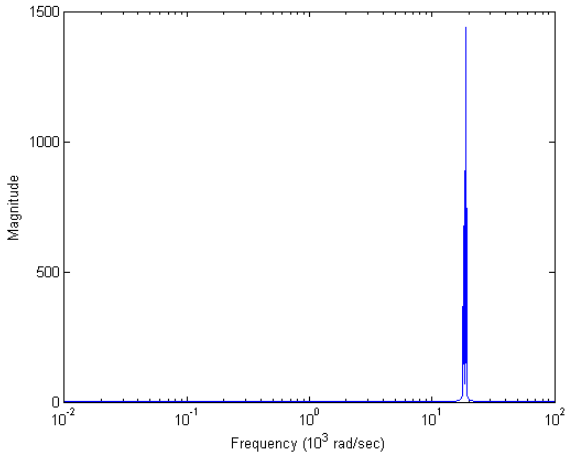

Figure 3.13: Structured singular value plot for the closed loop system of 5 cantilevers with the feedforward control

For the two parameters F and $\hat{F}$ a lagrangian equation is introduced which is minimized iteratively first with respect to F then with respect to $\hat{F}$, and calculating a new lagrange multiplier in each step.

The minimization process starts with an optimal unstructured feedback gain F_0 that is calculated through linear quadratic regulation. Because of the objective of having a good tracking performance rather than a mere regulation the system dynamics are augmented by an additional state q

$$q(t) = q(0) + \int_0^t (r - \hat{x}_1)dt \tag{3.21}$$

with r being the reference to track and $\hat{x}_1$ being the position state. So the

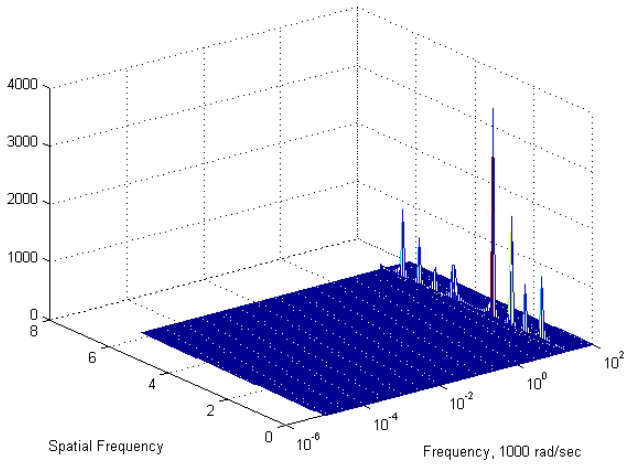

Figure 3.14: Structured singular value plot for the closed loop system with the feedforward control with infinite abstraction

system dynamics are rewritten in the following way:

$$\begin{bmatrix} \dot{\hat{x}} \\ \dot{q} \end{bmatrix} = \begin{bmatrix} A & 0 \\ -C_1 & 0 \end{bmatrix} \begin{bmatrix} \hat{x} \\ q \end{bmatrix} + \underbrace{\begin{bmatrix} 0 \\ 1 \end{bmatrix}}_{B1} r + \underbrace{\begin{bmatrix} B \\ 0 \end{bmatrix}}_{B2} u$$

$$\hat{x}_1 = C_1 \hat{x}$$

$$u = -F_0 \begin{bmatrix} \hat{x} \\ q \end{bmatrix} = \begin{bmatrix} -F_x & -F_q \end{bmatrix} \begin{bmatrix} \hat{x} \\ q \end{bmatrix} \tag{3.22}$$

The model of the above dynamical equations is shown in Figure 3.8 and the initial controller F_0 is calculated as a solution to the linear quadratic regulation for the above problem. The Q and R matrices are chosen in the following way:

$$q_d = \begin{bmatrix} 0 & 0 & 0 & 1 \end{bmatrix}$$

$$Q_d = 10^6 q_d' q_d \tag{3.23}$$

and the $4n \times 4n$ positive semidefinite matrix Q, where n represents the num-

ber of cantilevers, is:

$$Q = \begin{bmatrix} Q_d & 0_{4\times4} & \dots & 0_{4\times4} \\ 0_{4\times4} & Q_d & \dots & 0_{4\times4} \\ \vdots & & \ddots & \vdots \\ 0_{4\times4} & 0_{4\times4} & \dots & Q_d \end{bmatrix} \tag{3.24}$$

The positive definite matrix R is then

$$R = 10^{-9} I_n \tag{3.25}$$

with I_n being $n \times n$ identity matrix.

After applying some polishing steps the final controller can be obtained, having a distributed structure communicating with the immediate neighbors only.

3.3.2 Simulation of the Nonlinear System

Simulations are done with a 5 cantilever-nonlinear system. The reference input has a frequency of 1000 rad/sec with an amplitude of 10 nm for each cantilever. The tracking errors of all cantilevers are shown in Figure 3.15 and they are around 1 nm. The tracking error gets higher if the reference frequency is increased and reaches almost 3 nm at 3000 rad/sec, yielding worse performance than the previous feedforward control. However,unlike the feedforward control system,the tracking error doesn't increase significantly if the excitation frequency varies along the cantilever array, as seen in Figure 3.17. Figure 3.16 presents reference input along with the tracked output for two sample cantilevers.

The control effort has to be lower than certain limits. Figure 3.19 shows that the control effort is below $\pm 7V$.

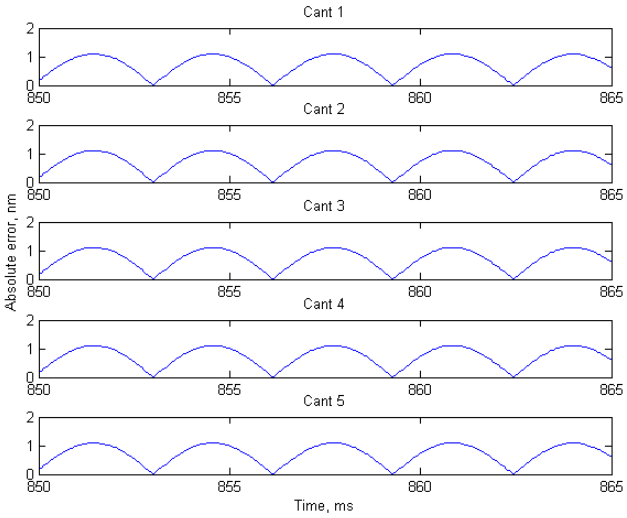

Figure 3.15: LQR Control design: Tracking error of 5 cantilevers. The excitation frequency and amplitude are 1000rad/sec and 10nm respectively

3.3.3 Stability and Robustness Analysis

As in the previous case, robust stability analysis is also performed for the LQR Controller. Figure 3.20 shows the sensitivity plot of the closed loop system according to which the LQR controller has a bandwidth of roughly 10000 rad/sec. Similarly, the LSTI abstraction yields the result Figure 3.21 which is very similar to Figure 3.20. This means that a model of 5 cantilevers is actually a satisfactory approximation of the actual infinite system. The LQR system has a tracking error of almost 2 nm at 2000 rad/sec and it increases further as the frequency is increased. However, unlike the feedforward control, instability is not observed at even very high frequencies.

The phase and gain margins are calculated for the LQR control that is implemented on the isolated single cantilever. The system with the controller has a phase margin of 60 degrees and a gain margin of 7.35 dB, as shown in Figure 3.22. The closed loop system is stable and both margins have more

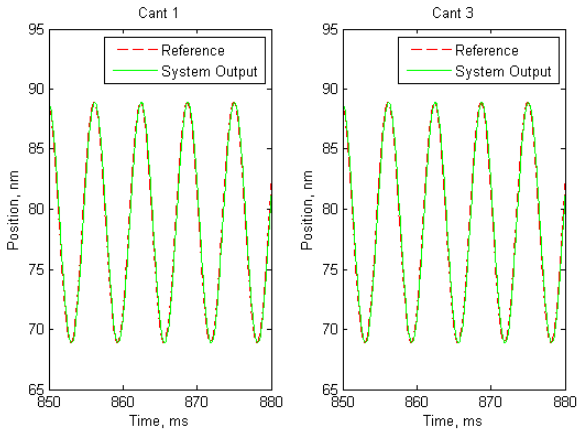

Figure 3.16: LQR Control design: Reference input and tracked output for two sample cantilevers. The excitation frequency and amplitude are 1000rad/sec and 10nm respectively

desirable values than the feedforward controller. This result is compatible with the relatively low peak value of the sensitivity plot of the closed loop system presented in Figure 3.20 indicating the high robustness of the system.

For further robustness analysis of the LQR control the structured singular value (SSV) is calculated, both for the finite 5 cantilever system and for the infinite abstraction. The same uncertainty structure with the same gains is used as described in equations 3.13 and 3.15. The plots can be seen in Figure 3.23 and Figure 3.24 for the finite and infinite models respectively. The magnitude of the SSV is significantly lower in comparison to the feedforward control although the same model is used. The result implies that the LQR controller's robustness properties are superior to the ones of the feedforward controller.

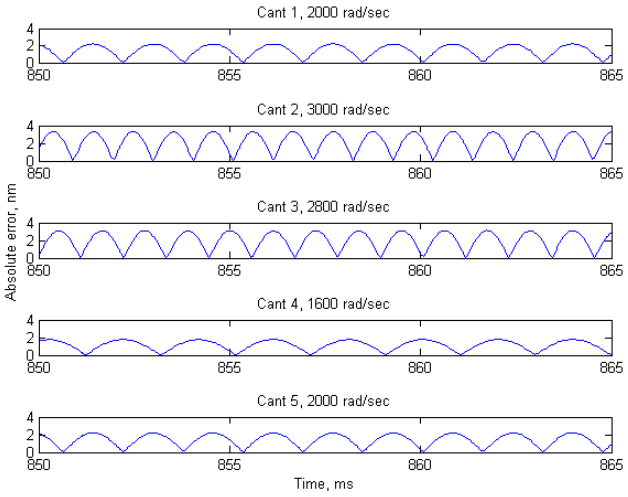

Figure 3.17: LQR Control design: Tracking error of 5 cantilevers at different excitation frequency

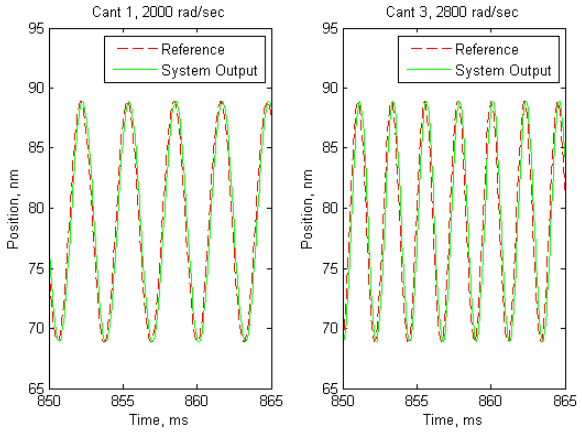

Figure 3.18: LQR Control design: Reference input and tracked output of two sample cantilevers at different excitation frequency

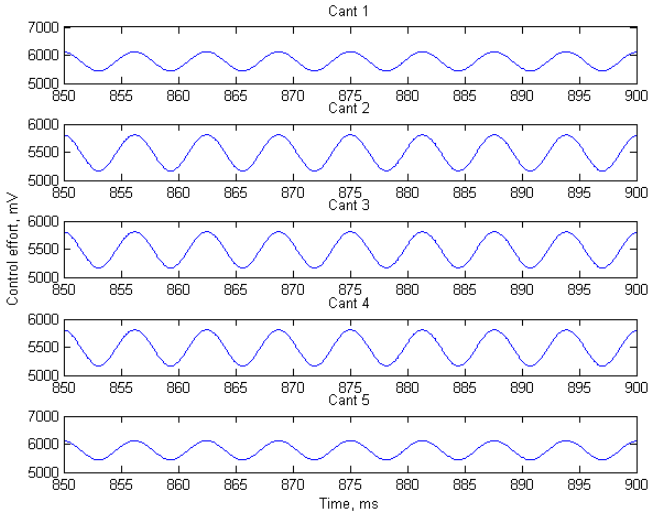

Figure 3.19: LQR Control design: Control effort of the cantilevers. The excitation frequency and amplitude are 1000rad/sec and 10nm respectively

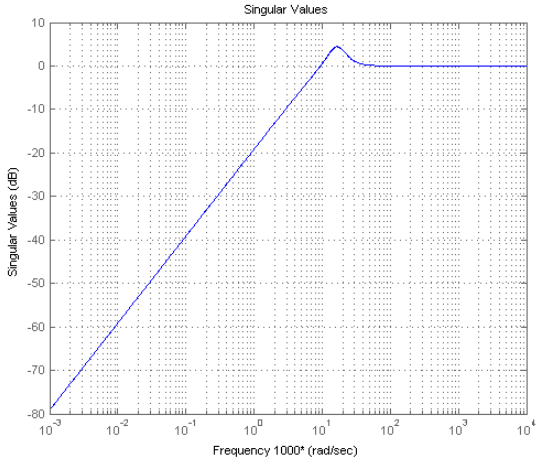

Figure 3.20: LQR Control design: Sensitivity Plot of the LQR Control System for an array of 5 cantilevers

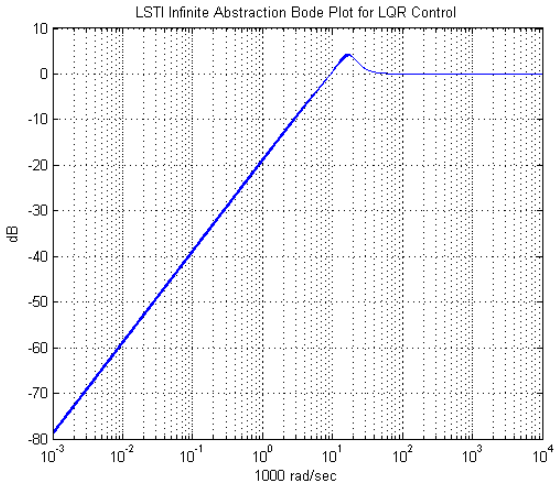

Figure 3.21: LQR Control design: LSTI Infinite Abstraction Bode Magnitude Plot

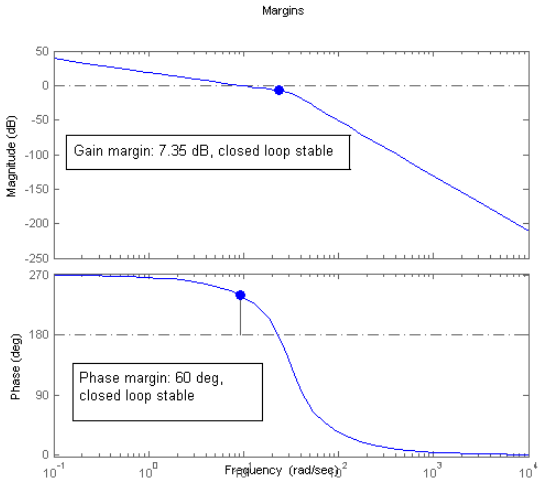

Figure 3.22: Phase and gain margins of the LQR Control System for an isolated cantilever

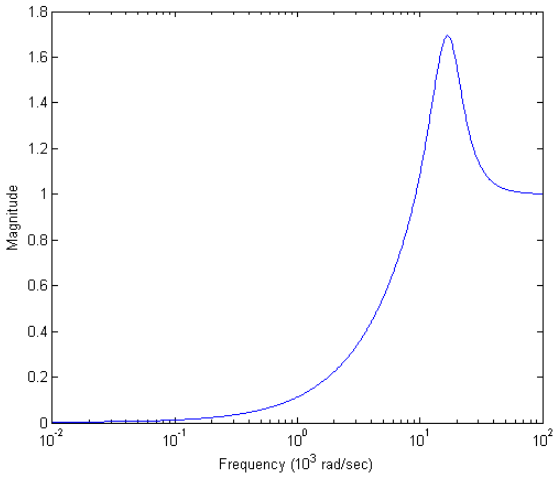

Figure 3.23: Structured singular value plot for the closed loop system of 5 cantilevers with the LQR control

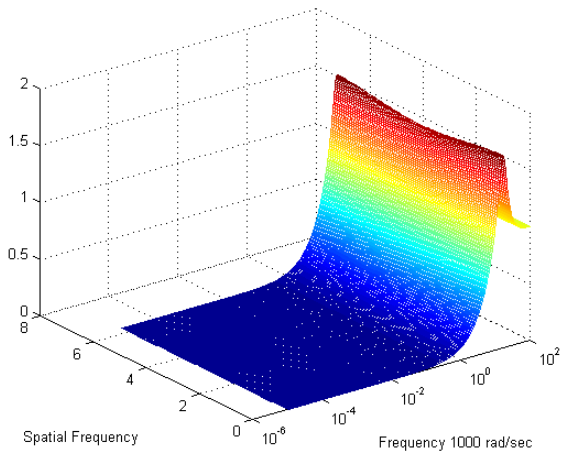

Figure 3.24: Structured singular value plot for the closed loop system with the LQR control designed using infinite abstraction

CHAPTER 4

CENTRALIZED H_∞ CONTROL

4.1 Introduction

The previously presented controllers require state information which may not always be available. Furthermore, although yielding satisfactory results and being easy to implement, the feedforward controller does not guarantee good tracking or even stability for frequencies higher than 4000 rad/sec, especially when there is a phase lag, while the LQR control already has a high tracking error at a frequency of 3000 rad/sec. In this chapter an ouput feedback H_∞ controller is therefore designed for a system of five cantilever array, in order to obtain an idea of the feasible performance under the ideal scenario of having a centralized architecture. Thus we will have some sort of benchmark performance index to compare with simpler and practically feasible schemes for large arrays such as the distributed controller in the following chapter. Furthermore this benchmark will be used in the multimodal design in chapter 6. The primary objective of the controller is to be able to independently track the reference input command issued at each cantilever. At the same time we want to minimize the effects of measurement noise, moisture and any possible wind present. Also, we seek a certain degree of robustness of our design to modelling errors and uncertainties. In this chapter first some theoretical background on H_∞ control from [17] and [18] is provided, later the control design and simulation results are presented.

4.2 H_∞ Control Theory

Feedback design problems can be cast as H_∞ design problems in many different ways. A standard problem formulation is afforded by the configuration shown in Figure 4.1 that is described by

$$\begin{bmatrix} z \\ y \end{bmatrix} = P \begin{bmatrix} w \\ u \end{bmatrix} = \begin{bmatrix} P_{11}(s) & P_{12}(s) \\ P_{21}(s) & P_{22}(s) \end{bmatrix} \begin{bmatrix} w \\ u \end{bmatrix}$$
$$u = K(s)y \tag{4.1}$$

with the generalized plant P having the state space realization

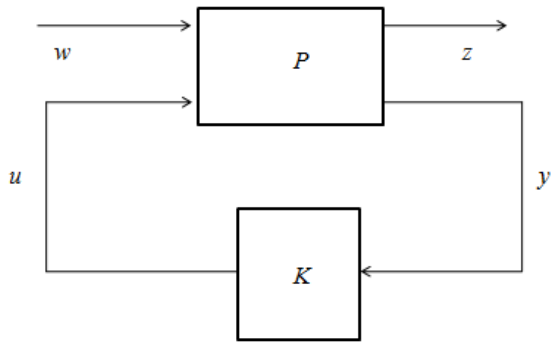

Figure 4.1: General Control Configuration

$$P(s) = \begin{bmatrix} A & B_1 & B_2 \\ C_1 & D_{11} & D_{12} \\ C_2 & D_{21} & D_{22} \end{bmatrix} \tag{4.2}$$

The signals are: u the control variables, y the measured variables, w the exogenous signals such as disturbances or commands, and z the variables to be minimized to meet the control objectives, typically the error signals. The closed loop transfer function from w to z is given by the linear fractional transformation

$$z = F_l(P, K)w \tag{4.3}$$

where

$$F_l(P,K) = P_{11} + P_{12}K(I - P_{22}K)^{-1}P_{21} \tag{4.4}$$

The objective of the control problem is minimizing the H_∞ norm of $F_l(P,K)$

The essential assumptions for the H_∞ control problem are the following:

1. (A, B_2) is stabilizable and (C_2, A) is detectable;
2. D_{12} and D_{21} have full rank (for simplicity: $D_{12} = \begin{bmatrix} 0 \\ I \end{bmatrix}$ and $D_{21} = \begin{bmatrix} 0 & I \end{bmatrix}$);
3. $\begin{bmatrix} A - j\omega I & B_2 \\ C_1 & D_{12} \end{bmatrix}$ has full column rank for all ω;
4. $\begin{bmatrix} A - j\omega I & B_1 \\ C_2 & D_{21} \end{bmatrix}$ has full row rank for all ω;

The following definitions are made:

$$R := D_{1\bullet}^* D_{1\bullet} - \begin{bmatrix} \gamma^2 I_{m1} & 0 \\ 0 & 0 \end{bmatrix} \text{ where } D_{1\bullet} := \begin{bmatrix} D_{11} & D_{12} \end{bmatrix}$$

$$\tilde{R} := D_{\bullet 1}^* D_{\bullet 1} - \begin{bmatrix} \gamma^2 I_{p1} & 0 \\ 0 & 0 \end{bmatrix} \text{ where } D_{\bullet 1} := \begin{bmatrix} D_{11} \\ D_{21} \end{bmatrix}$$

$$H_\infty := \begin{bmatrix} A & 0 \\ -C_1^* C_1 & -A^* \end{bmatrix} - \begin{bmatrix} B \\ -C_1^* D_{1\bullet} \end{bmatrix} R^{-1} \begin{bmatrix} D_{1\bullet}^* C_1 & B^* \end{bmatrix}$$

$$J_\infty := \begin{bmatrix} A^* & 0 \\ -B_1 B_1^* & -A \end{bmatrix} - \begin{bmatrix} C^* \\ -B_1 D_{\bullet 1}^* \end{bmatrix} \tilde{R}^{-1} \begin{bmatrix} D_{\bullet 1} B_1^* & C \end{bmatrix}$$

$X_\infty = Ric(H_\infty)$; $Y_\infty = Ric(J_\infty)$

$$F := \begin{bmatrix} F_{1\infty} \\ F_{2\infty} \end{bmatrix} := -R^{-1}[D_{1\bullet}^* C_1 + B^* X_\infty]$$

$$L := \begin{bmatrix} L_{1\infty} & L_{2\infty} \end{bmatrix} := -[B_1 D_{\bullet 1}^* + Y_\infty C^*]\tilde{R}^{-1}$$

Theorem 2. *Suppose P satisfies the assumptions 1-4.*

1. *There exists an admissable controller $K(s)$ such that $\|F_l(P,K)\|_\infty < \gamma$ (i.e., $\|T_{zw}\|_\infty < \gamma$) if and only if*

   (a) $\gamma > max(\bar{\sigma}[D_{1111}, D_{1112}], \bar{\sigma}[D^*_{1111}, D^*_{1121}])$

   (b) $H_\infty \in dom(Ric)$ *with* $X_\infty = Ric(H_\infty) \geq 0$

   (c) $J_\infty \in dom(Ric)$ *with* $Y_\infty = Ric(J_\infty) \geq 0$

   (d) $\rho(X_\infty Y_\infty) < \gamma^2$

2. *Given that the conditions of part(1) are satisfied, then all rational internally stabilizing controllers $K(s)$ satisfying $\|F_l(P,K)\|_\infty < \gamma$ are given by*

   $K = F_l(M_\infty, Q)$ *for arbitrary $Q \in RH_\infty$ such that $\|Q\|_\infty < \gamma$ where*

$$M_\infty = \begin{bmatrix} \hat{A} & \hat{B}_1 & \hat{B}_2 \\ \hat{C}_1 & \hat{D}_{11} & \hat{D}_{12} \\ \hat{C}_2 & \hat{D}_{21} & 0 \end{bmatrix}$$

$$\hat{D}_{11} = -D_{1121} D^*_{1111} (\gamma^2 I - D_{1111} D^*_{1111})^{-1} D_{1112} - D_{1122}$$

   $\hat{D}_{12} \in \mathcal{R}^{m_2 \times m_2}$ *and* $\hat{D}_{21} \in \mathcal{R}^{p_2 \times p_2}$ *are any matrices satisfying*

$$\hat{D}_{12} \hat{D}^*_{12} = I - D_{1121} (\gamma^2 I - D^*_{1111} D_{1111})^{-1} D^*_{1112}$$
$$\hat{D}^*_{21} \hat{D}_{21} = I - D^*_{1112} (\gamma^2 I - D_{1111} D^*_{1111})^{-1} D^*_{1112}$$

   and

$$\hat{B}_2 = Z_\infty (B_2 + L_{12\infty}) \hat{D}_{12}$$
$$\hat{C}_2 = -\hat{D}_{21} (C_2 + F_{12\infty})$$
$$\hat{B}_1 = -Z_\infty L_{2\infty} + \hat{B}_2 \hat{D}^{-1}_{12} \hat{D}_{11}$$
$$\hat{C}_1 = F_{2\infty} + \hat{D}_{11} \hat{D}^{-1}_{21} \hat{C}_2$$
$$\hat{A} = A + BF + \hat{B}_1 \hat{D}^{-1}_{21} \hat{C}_2$$

   where

$$Z_\infty = (I - \gamma^{-2} Y_\infty X_\infty)^{-1}$$

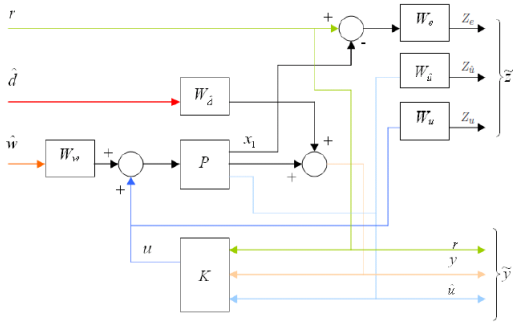

Figure 4.2: LFT Formulation for H_∞ Control Design

4.3 Control Design

In this section a suboptimal H_∞ centralized controller is designed for a small array of five microcantilevers, leveraging on the work in [9]. The controller is designed by adding disturbance to each cantilever through the input channel, sensor noise in the output channel of each cantilever and by introducing controlled outputs of each cantilever's tracking error, input voltage and rate of change of the input voltage. The dynamics of the additional artificial disturbances,noises and controlled outputs on one cantilever are derived as follows. Define the state matrix

$$A_{uc} = \begin{bmatrix} 0 & 1 & 0 \\ -\frac{\omega^2}{\omega_0^2} + \frac{\epsilon_0 A V_e^2}{\omega_0^2 m d^3 \delta_V^2} & -\frac{b}{\omega_0} & \frac{\delta_x}{\delta_V}\left(\frac{2\hat{x}_{e1}\epsilon_0 A \hat{V}_e}{m d^3 \omega_0^2 \delta_V^2} + \frac{\epsilon_0 A \hat{V}_e}{m d^2 \omega_0^2}\right) \\ 0 & 0 & 0 \end{bmatrix}$$

defining $\bar{y}_i = \begin{bmatrix} \hat{y}_i \\ \hat{u} \end{bmatrix}$ where $\hat{u} = \hat{V}_i$, the state space equations can be written as

$$\dot{\hat{x}}_i = A_{uc}\hat{x}_i + \tilde{B}\dot{\hat{V}}_i + \bar{B}\hat{w}_i$$

$$\bar{y}_i = \tilde{C}\hat{x}_i + \tilde{D}\dot{\hat{V}}_i + W_{\hat{d}}\hat{d}_i$$

where $\hat{w}_i = \sum_{j=-\infty, j\neq i}^{\infty} \hat{G}_{i-j}\hat{x}_j$, $\bar{B} = \begin{bmatrix} 0 \\ W_w \\ 0 \end{bmatrix}$, $\tilde{C} = \begin{bmatrix} 0 & \frac{\hat{V}_e \epsilon_0 A}{d^2} & 0 \\ 0 & 0 & 1 \end{bmatrix}$ and $\tilde{D} = \begin{bmatrix} \frac{\delta_x}{\delta_v}\omega_0 \left(\frac{\epsilon_0 A}{d} + \frac{\epsilon_0 A \hat{x}_{e1}}{d^2}\right) \\ 0 \end{bmatrix}$, with $\hat{d}_i$ and $W_{\hat{d}}$ as the sensor noise and the corresponding weight on it. The framework for the linear fractional transformation (LFT) of the system can be seen in Figure 4.2, where P is the given plant and K is the designed controller. Neglecting the index i we define $\tilde{y} = \begin{bmatrix} \bar{y} \\ r \end{bmatrix}$; $\tilde{z} = \begin{bmatrix} \tilde{r} - \tilde{x}_1 \\ \tilde{u} \\ \bar{u} \end{bmatrix}$; $\tilde{w} = \begin{bmatrix} \hat{w} \\ \hat{d} \\ r \end{bmatrix}$; $u = \dot{\hat{V}}$ and $\tilde{u} = W_u \dot{\hat{V}}$; $\bar{u} = W_{\hat{u}}\hat{u}$; thus we can write,

$$\dot{\hat{x}} = A_{uc}\hat{x} + \begin{bmatrix} \bar{B} & 0_{3\times 2} & \begin{bmatrix} 0 \\ 0 \\ 1 \end{bmatrix} \end{bmatrix} \cdot \begin{bmatrix} \hat{w} \\ \hat{d} \\ r \\ u \end{bmatrix}$$

$$\tilde{z} = \begin{bmatrix} -W_e & 0 & 0 \\ 0 & 0 & 0 \\ 0 & 0 & W_{\hat{u}} \end{bmatrix} \cdot \hat{x} + \begin{bmatrix} 0 & 0 & W_e & 0 \\ 0 & 0 & 0 & W_u \\ 0 & 0 & 0 & 0 \end{bmatrix} \cdot \begin{bmatrix} \hat{w} \\ \hat{d} \\ r \\ u \end{bmatrix}$$

$$\tilde{y} = \begin{bmatrix} \tilde{C} \\ 0_{1\times 3} \end{bmatrix} \cdot \hat{x} + \begin{bmatrix} 0_{2\times 1} & \begin{bmatrix} W_d \\ 0 \end{bmatrix} & 0_{2\times 1} & \tilde{D} \\ 0 & 0 & 1 & 0 \end{bmatrix} \cdot \begin{bmatrix} \hat{w} \\ \hat{d} \\ r \\ u \end{bmatrix}$$

The following weights are assumed to begin the analysis: $W_u = \rho_1$, $W_{\hat{u}} = \rho_2$ are to be chosen so that the control effort and its rate of change are minimized.

$W_{\hat{d}} = \frac{K_1}{s+\epsilon_1}$; where K_1 and ϵ_1 are chosen such that the effect of high frequency measurement noise on the system output is attenuated. $W_e = K_2\frac{s+a_1}{s+\epsilon_2}$; where K_2, a_1 and ϵ_2 should be adjusted in order to minimize the tracking error at low frequencies. $W_w = \epsilon_3$ should be chosen so that the effect of any external disturbance, entering the system at the input channel, is attenuated. $\{\rho_1, \rho_2, \epsilon_1, \epsilon_2, K_1, K_2, a_1\} \in R$ are design parameters to be chosen so that the performance requirements are met. The dynamics of W_e can be written state space form as follows

$$\dot{\hat{x}}_4 = -\epsilon_2\hat{x}_4 + r - \hat{x}_1$$
$$\tilde{e} = \tilde{r} - \tilde{x}_1 = K_2(a_1 - \epsilon_2)\hat{x}_4 + K_2(r - \hat{x}_1)$$

where

$$e = r - \hat{x}_1$$

Similarly the state space realization for the dynamics of $W_{\hat{d}}$ can be written as follows;

$$\dot{\hat{x}}_5 = -\epsilon_1\hat{x}_5 + K_1\hat{d}$$
$$\hat{y} = \frac{\hat{V}_e\epsilon_0 A}{d^2}\hat{x}_2 + \hat{x}_5 + \frac{\delta_x}{\delta_v}\omega_0\left(\frac{\epsilon_0 A}{d} + \frac{\epsilon_0 A\hat{x}_{e1}}{d^2}\right)u$$

Using the above state space realization in our system realization we can

write as follows:

$$\dot{\hat{x}} = \underbrace{\begin{bmatrix} \begin{bmatrix} A_{uc} & 0_{3\times1} \end{bmatrix} & 0_{3\times1} \\ \begin{bmatrix} -1 & 0 & 0 & -\epsilon_2 \end{bmatrix} & 0 \\ 0_{1\times4} & -\epsilon_1 \end{bmatrix}}_{A_{big}} \cdot\hat{x} + \underbrace{\begin{bmatrix} & & & \begin{bmatrix} 0 \\ 0 \\ 1 \end{bmatrix} \\ \epsilon_2\bar{B} & 0_{3\times1} & 0_{3\times1} & \\ 0 & 0 & 1 & 0 \\ 0 & K_1 & 0 & 0 \end{bmatrix}}_{B_{big}} \cdot \begin{bmatrix} \hat{w} \\ \hat{d} \\ r \\ u \end{bmatrix}$$

$$\tilde{z} = \underbrace{\begin{bmatrix} -K_2 & 0 & 0 & K_2(a_1-\epsilon_2) \\ 0 & 0 & 0 & 0 \\ 0 & 0 & \rho_2 & 0 \end{bmatrix}}_{C_{big1}} \cdot\hat{x} + \underbrace{\begin{bmatrix} 0 & 0 & K_2 & 0 \\ 0 & 0 & 0 & \rho_1 \\ 0 & 0 & 0 & 0 \end{bmatrix}}_{D_{big1}} \cdot \begin{bmatrix} \hat{w} \\ \hat{d} \\ r \\ u \end{bmatrix}$$

$$\tilde{y} = \underbrace{\begin{bmatrix} \tilde{C} & 0_{2\times1} & \begin{bmatrix} 1 \\ 0 \end{bmatrix} \\ 0_{1\times3} & 0 & 0 \end{bmatrix}}_{C_{big2}} \cdot\hat{x} + \underbrace{\begin{bmatrix} 0_{2\times2} & 0_{2\times1} & \tilde{D} \\ 0_{1\times2} & 1 & 0 \end{bmatrix}}_{D_{big2}} \cdot \begin{bmatrix} \hat{w} \\ \hat{d} \\ r \\ u \end{bmatrix}$$

The model system consists of five cantilevers. The augmented system dynamics can thus be written as:

$$\dot{\hat{x}}_c = A_c\hat{x}_c + B_c \begin{bmatrix} w_c & d_c & r_c & u_c \end{bmatrix}' \tag{4.5}$$

$$\tilde{z}_c = C_{1c}\hat{x}_c + D_{1c} \begin{bmatrix} w_c & d_c & r_c & u_c \end{bmatrix}' \tag{4.6}$$

$$\tilde{y}_c = C_{2c}\hat{x}_c + D_{2c} \begin{bmatrix} w_c & d_c & r_c & u_c \end{bmatrix}' \tag{4.7}$$

with $\hat{x}_c$ being the vector of the states of 5 cantilevers, each having augmented dynamics, $\tilde{z}$ and $\tilde{y}$ the corresponding vectors for the variables to be minimized

and measured variables respectively, and

$$A_c = \begin{bmatrix} \hat{A}_{big} & EM & E_1 & E_2 & E_3 \\ EM & \hat{A}_{big} & EM & E_1 & E_2 \\ E_2 & E_M & \hat{A}_{big} & E_M & E_1 \\ E_3 & E_2 & E_1 & E_M & \hat{A}_{big} \end{bmatrix} \tag{4.8}$$

where

$$\hat{A}_{big} = \begin{bmatrix} \begin{bmatrix} \hat{A}_{uc} & 0_{3\times1} \end{bmatrix} & 0_{3\times1} \\ \begin{bmatrix} -1 & 0 & 0 & -\epsilon_2 \end{bmatrix} & 0 \\ 0_{1\times4} & -\epsilon_1 \end{bmatrix} \tag{4.9}$$

and

$$\begin{aligned} \hat{A}_{uc} &= A_{uc} + \begin{bmatrix} 0 & 0 & 0 \\ E_0 + M_0 & 0 & 0 \\ 0 & 0 & 0 \end{bmatrix} \\ E_0 &= \left(1 + \frac{\hat{x}_{e1}^2}{d^2\delta_x^2} + \frac{2\hat{x}_{e1}}{d\delta_x}\right) \epsilon_0 \frac{A^2\hat{V}_e^2}{d^2 m 4\pi\omega_0^2\delta_V^2} \sum_{j=-\infty, j\neq i}^{\infty} \frac{1}{r_{i,j}^3} \\ M_0 &= -\frac{1}{m\omega_0^2} \sum_{j=i-1, j\neq i}^{i+1} \gamma_{i,j} \end{aligned} \tag{4.10}$$

EM is the sum of the mechanical and electrical couplings from the immediate neighbors and E_i are the electrical couplings from the further neighbors. C_{1c} and C_{2c} consist of five diagonally augmented matrices of C_{big1} and C_{big2} respectively. In order to create D_{1c} each column of D_{big1} is diagonally augmented five times so that the equations hold for $w_c = \left[\hat{w}_{5\times1}\right]$, $d_c = \left[\hat{d}_{5\times1}\right]$, $r_c = \left[r_{5\times1}\right]$, $u_c = \left[u_{5\times1}\right]$. B_c and D_{2c} are obtained in the same way as D_{1c} from B_{big} and D_{big1} respectively.

Using the MATLAB Robust Control Toolbox the H_∞ controller is de-

signed:

$$\dot{x}_k = A_k x_k + B_k y$$

$$u = C_k x_k + D_k y$$

having 25 states for a 5 cantilever system.

In order to satisfy certain conditions for the H_∞ design and in order to have a small tracking error along with a low control effort the following weights are used: $W_u = 0.0025$, $W_{\hat{u}} = 2.3$, $W_w = 2.7$, $W_e = 34\frac{s+7000002}{s+0.0041}$, $W_{\hat{d}} = \frac{4}{s+100}$. The Bode plots of W_e and $W_{\hat{d}}$ can be seen in Figure 4.3 and Figure 4.4.

4.4 Simulations

This section shows results of the simulations carried out with the Matlab software. The controller was tested on a model consisting of five cantilevers and the whole array of cantilevers having one centralized controller. The reference input has a frequency of 3000 rad/sec with an amplitude of 10 nm for each cantilever. The absolute tracking error of the cantilevers is presented in Figure 4.5. Also the comparison between the reference input and the tracked output for two sample cantilevers is shown in Figure 4.6. The absolute tracking error is around 1 nm, less than 2 nm. It could be expected that the performance is worse than the previous feedforward controller, since this controller doesn't have the full state information, although being centralized. Besides its performance is significantly better than the feedforward controller if the frequencies along the cantilever array vary, as seen in Figure 4.7 where the tracking errors are all less than 2 nm. As seen in Figure 4.9 the control effort for each cantilever is below 4 V, much lower than the one for the feedforward control system.

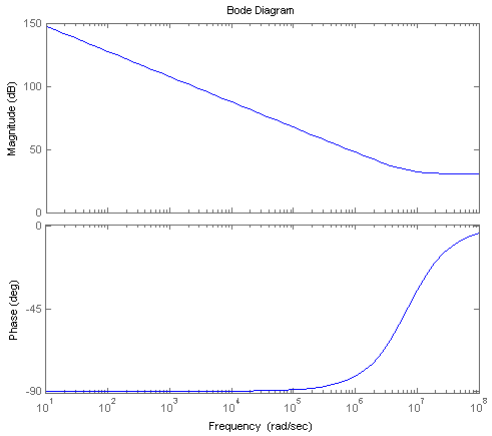

Figure 4.3: Bode Plot for W_e

4.5 Stability and Robustness Analysis

Stability analysis of the closed loop centralized H_∞ control system is performed in this section. Figure 4.10 shows the sensitivity plot of the system having a bandwidth of 40000 rad/sec. The complementary sensitivity function seen in 4.10 has the same bandwidth as well. This value is significantly higher than the bandwidths of the feedforward and LQR control systems. Although being an output feedback system this result is expected since the centralized H_∞ controller receives all the output and coupling information. The simulations show that the tracking error is approximately 2 nm at a frequency of 5000 rad/sec and the system doesn't become unstable at frequencies as high as 30000 rad/sec. The simulations thus verify the superior tracking performance of the centralized H_∞ control which is going to be a benchmark for the distributed H_∞ controller presented in the next chapter.

For further robustness analysis of the centralized H_∞ control the structured singular value (SSV) is calculated for the finite 5 cantilever system. The same uncertainty structure with the same gains is used as described in equations

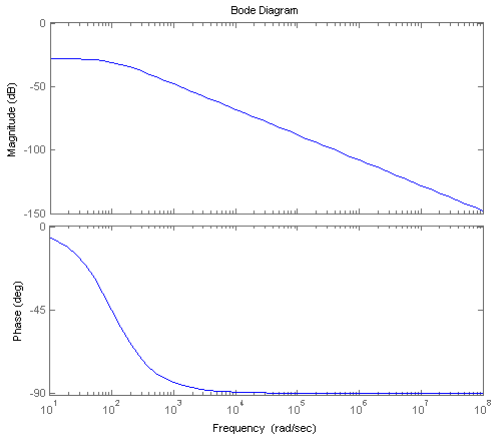

Figure 4.4: Bode Plot for W_d

3.13 and 3.15. The SSV plot can be seen in Figure 4.12. The SSV has a peak magnitude at around 10000 rad/sec and is significantly lower in the remaining frequency regions. The peak value is lower than the one of the feedforward control but higher than the one of the LQR control. Despite this fact a comparison of the output feedback, centralized H_∞ control with the state feedback feedforward and LQR controllers in terms of SSV analysis may not provide accurate results because of the lack of state information of the H_∞ control system. Therefore we are only going to claim that the SSV results of the centralized controller of this chapter are providing a benchmark for the robustness of the distributed H_∞ control presented next.

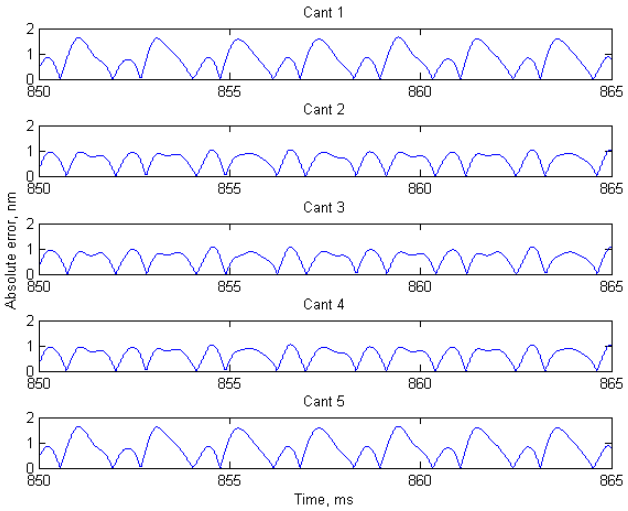

Figure 4.5: Centralized H_∞ Control Design: Tracking error for the system of 5 cantilevers at the excitation frequency of 3000 rad/sec and 10 nm amplitude

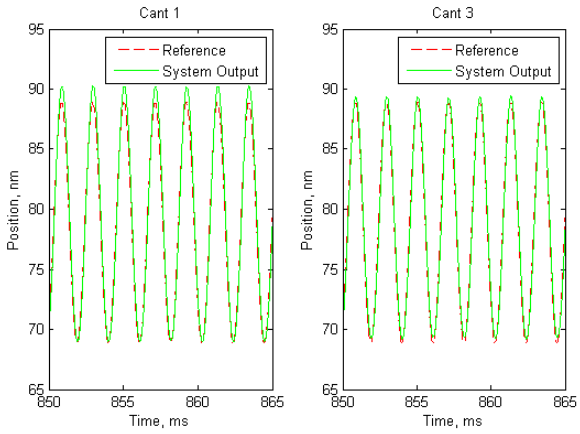

Figure 4.6: Centralized H_∞ Control Design: Reference input and tracked output for two sample cantilevers. Reference frequency is 3000 rad/sec and the amplitude is 10 nm

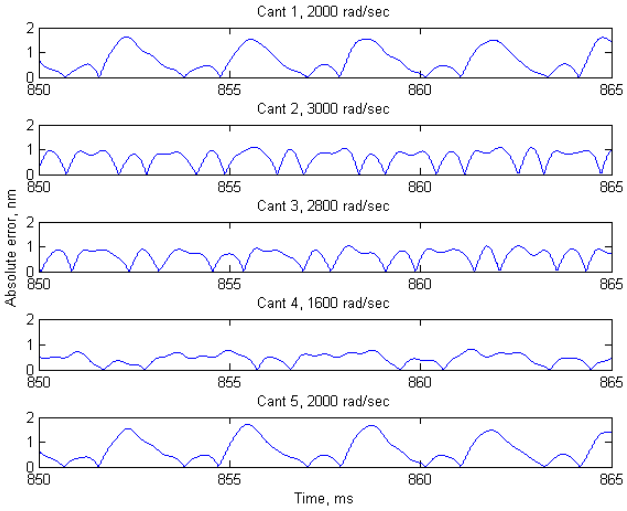

Figure 4.7: Centralized H_∞ Control Design: Tracking error for the system of 5 cantilevers at different excitation frequencies

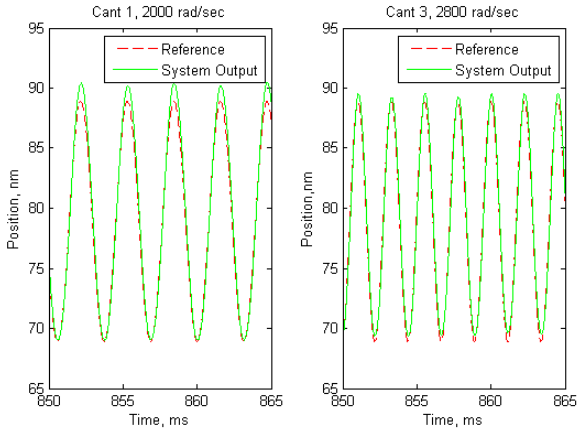

Figure 4.8: Centralized H_∞ Control Design: Reference input and tracked output for two sample cantilevers at different excitation frequencies

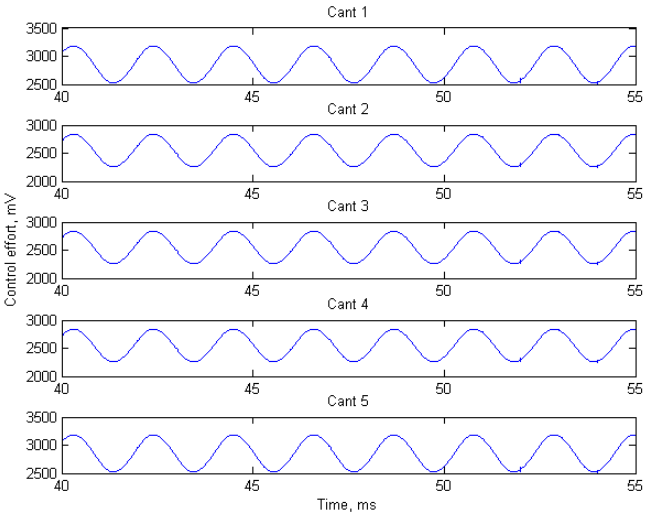

Figure 4.9: Centralized H_∞ Control Design: Sample control effort for five cantilever system. The excitation frequency and amplitude are 3000rad/sec and 10nm respectively

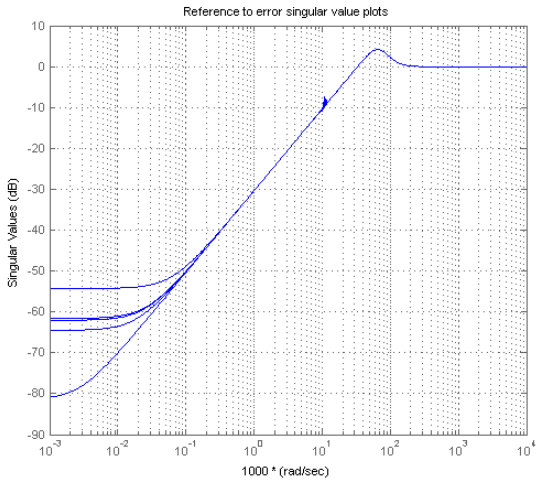

Figure 4.10: Singular Value Plot of Reference to Error Transfer Function Using a Centralized H_∞ Control

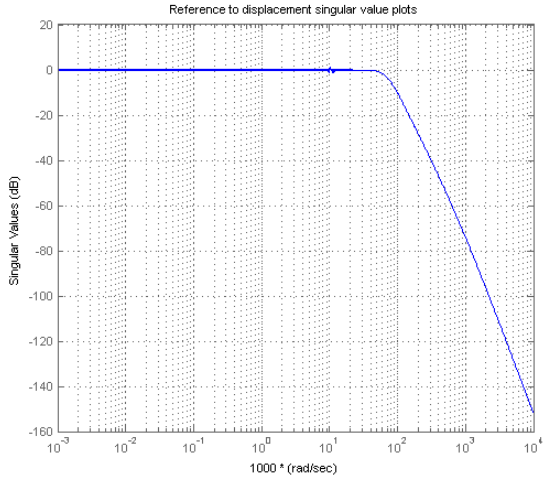

Figure 4.11: Singular Value Plot of Reference to Displacement Transfer Function Using a Centralized H_∞ Control

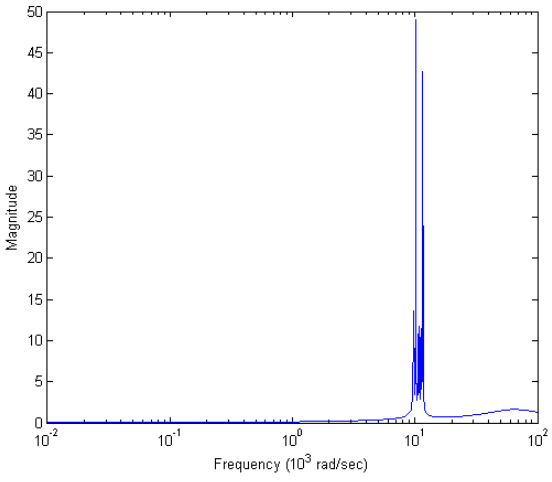

Figure 4.12: Structured singular value plot for the closed loop system of 5 cantilevers with the centralized H_∞ control

CHAPTER 5

DISTRIBUTED H_∞ CONTROL

5.1 Introduction

The centralized H_∞ controller cannot be implemented on large distributed systems consisting of hundreds of segments. With their ease of implementation, requiring merely the information from a single cantilever and its local neighborhood, distributed controllers are more suitable for such systems. The cantilever system we are considering is assumed to have an infinite one dimensional array of identical cantilevers that carry identical control elements. This spatial invariance is a significant simplification to the control design. In Chapter 3 two kinds of localized controllers were implemented both of which used the state information. The objective of this chapter is to design a localized, distributed H_∞ controller, using only the output information of the single cantilever, communicating with the controllers in the immediate neighborhood and achieving the performance of the centralized controller. The findings from [19] have a significant contribution to the distributed H_∞ control design for spatially invariant systems that can be described as as distribution of a linear time invariant (LTI) system over a spatial frequency parameter θ. The theorems in [19] state that the whole system is stable (stabilizable) if stability (stabilizability) can be achieved for every θ. The cantilever array considered in this thesis consists of infinitely many cantilevers with the same dynamics and therefore, with the help of the above result, the

LSTI abstraction and stability analysis of one isolated cantilever are going to provide results about the stability of the whole system

5.2 Distributed H_∞ Control Theorem

From the mathematical background about the spatial invariance and stability of distributed systems provided in [19] a controller for such systems can be introduced. The generalized plant is a space/time invariant, distributed system and its linear approximation admits a state space representation. The feedback controller is also going to be distributed and must both stabilize the system and minimize a certain norm of the closed loop map T_{zw}. Under these circumstances the closed loop $H := T_{zw}$ is a space and time invariant system having the following transfer function description:

$$\hat{z}(\lambda, s) = \hat{H}(\lambda, s)\hat{w}(\lambda, s) \tag{5.1}$$

having the same structure as in Figure 4.1 only with the addition of the spatial operator λ.

For the H_∞ optimization the state space description of the plant can be written as follows if the spatial operator λ is omitted

$$\begin{aligned} \frac{\partial}{\partial t}x(.,t) &= Ax(.,t) + B_1 w(.,t) + B_2 u(.,t) \\ z(.,t) &= C_1 x(.,t) + D_{12} u(.,t) \\ y(.,t) &= C_2 x(.,t) + D_{21} w(.,t) \end{aligned} \tag{5.2}$$

The design problem is to find the controller of the form:

$$\begin{aligned} \frac{\partial}{\partial t}x_k(.,t) &= A_k x_k(.,t) + B_k y(.,t) \\ u(.,t) &= C_k x_k(.,t) + D_k y(.,t) \end{aligned} \tag{5.3}$$

such that the closed loop system is exponentially stable and $\|T_{zw}\|_\infty < 1$. The fourier transform of 5.2 is:

$$\begin{aligned}
\frac{\partial}{\partial t}x_\lambda(.,t) &= \hat{A}_\lambda x_\lambda(.,t) + \hat{B}_{1,\lambda}\hat{w}(.,t) + \hat{B}_{2,\lambda}\hat{u}(.,t) \\
\hat{z}_\lambda(.,t) &= \hat{C}_{1,\lambda}x(.,t) + \hat{D}_{12,\lambda}\hat{u}(.,t) \\
\hat{y}_\lambda(.,t) &= \hat{C}_{2,\lambda}x_\lambda(.,t) + \hat{D}_{21,\lambda}\hat{w}(.,t)
\end{aligned} \tag{5.4}$$

The system is thus reduced to a parameterized family of finite dimensional LTI systems over $\lambda \in \hat{\mathbb{G}}$. The H_∞ feasibility question$\|T_{wz}\|_\infty < 1$ can be imposed as a family of standard H_∞ conditions $\|T_{wz}(\lambda,\cdot)\|_\infty < 1$

Theorem 3. *Under the following regulating conditions,*

1. $\sigma_{min}\begin{bmatrix}\hat{A}(\lambda) - j\omega I & \hat{B}_2(\lambda) \\ \hat{C}_1(\lambda) & \hat{D}_{12}(\lambda)\end{bmatrix} \geq \epsilon > 0$
2. $\hat{D}_{12}(\lambda)\hat{D}_{12}^*(\lambda) \geq \epsilon I > 0 \quad \forall\lambda$
3. $\sigma_{min}\begin{bmatrix}\hat{A}(\lambda) - j\omega I & \hat{B}_1(\lambda) \\ \hat{C}_2(\lambda) & \hat{D}_{21}(\lambda)\end{bmatrix} \geq \epsilon > 0$
4. $\hat{D}_{21}\hat{D}_{21}^* \geq \epsilon I > 0$
5. (A, B_2) *and* (A^*, C_2^*) *are stabilizable.*

There exists an admissable controller if and only if the following three conditions are satisfied:

1. *For all* $\lambda \in \hat{G}$*, the matrix*

   $$H_1(\lambda) := \begin{bmatrix}\hat{A}(\lambda) & -(\hat{B}_1(\lambda)\hat{B}_1^*(\lambda) - \hat{B}_2(\lambda)\hat{B}_2^*(\lambda)) \\ -\hat{C}_1^*(\lambda)\hat{C}_1(\lambda) & -\hat{A}^*(\lambda)\end{bmatrix} \in dom(Ric),$$

   and the solution $\hat{P}_1(\lambda) := Ric(H_1(\lambda))$ *is bounded, i.e.* $sup_{\lambda\in\hat{\mathbb{G}}}\|\hat{P}_1(\lambda)\| < \infty$.

2. *For all* $\lambda \in \hat{G}$*, the matrix*

   $$H_2(\lambda) := \begin{bmatrix}\hat{A}^*(\lambda) & -(\hat{C}_1^*(\lambda)\hat{C}_1(\lambda) - C_2^*(\lambda)\hat{C}_2(\lambda)) \\ -\hat{B}_1(\lambda)\hat{B}_1^*(\lambda) & -\hat{A}(\lambda)\end{bmatrix} \in dom(Ric),$$

   and the solution $\hat{P}_2(\lambda) := Ric(H_2(\lambda))$ *is bounded, i.e.* $sup_{\lambda\in\hat{\mathbb{G}}}\|\hat{P}_2(\lambda)\| < \infty$.

3.

$$sup_{\lambda \in \hat{\mathbb{G}}} \rho(\hat{P}_1(\lambda)\hat{P}_2(\lambda)) < 1$$

where $\rho(\cdot)$ denotes spectral radius. In this case, one such controller is given by

$$\tilde{K} = \begin{bmatrix} A + (B_1 B_1^* - B_2 B_2^*)P_1 - Z P_2 C_2^* C_2 & Z P_2 C_2^* \\ -B_2^* P_1 & 0 \end{bmatrix}$$

where P_1, P_2 are the translation-invariant operators whose Fourier representations are $\{\hat{P}_1(\lambda)\}$, $\{\hat{P}_2(\lambda)\}$. $Z = (I - P_2 P_1)^{-1}$.

5.3 Distributed Control Design

In this section the distributed H_∞ controller is designed for the cantilever array. This is done by considering one cantilever and adding the information from the neighbors and considering the whole array dynamics by implementing the LSTI infinite approximation that is defined in Chapter 3. However before doing the LSTI approximation the single cantilever dynamics are augmented by artificial disturbances and controlled outputs in order to satisfy certain assumptions needed in the H_∞ software, as in Chapter 4. The model for the augmented dynamics can be seen in Figure 4.2 in Chapter 4 and the weights are W_u for penalizing the control effort, $W_{\hat{u}}$ to penalize the variation rate of the control effort, W_e as a penalty on the tracking error to achieve good tracking at low frequencies and $W_{\hat{d}}$ for attenuation of noise effects at high frequencies. A_{big}, B_{big}, C_{big} and D_{big} are the state, input, output and feedthrough matrices of the augmented single cantilever.

The LSTI approximation is conducted by using the shift operator $S = e^{j\theta}$ over the interval $[0, 2\pi]$, meaning $\theta \in [0, 2\pi]$. Assuming that the information of only 3 neighbors on each side is considerable the equation for the

augmented state matrix with the shift operator can be written as follows

$$A_{big}(S) = A_{big-3}S^{-3}+A_{big-2}S^{-2}+A_{big-1}S^{-1}+A_{big}+A_{big1}S^{1}+A_{big2}S^{2}+A_{big3}S^{3} \tag{5.5}$$

with $S^k = e^{kj\theta}$. The gridding is then done over the Fourier frequencies θ in order to get the infinite model for the controller design. By splitting C_{big} and D_{big} into C_{big1} and D_{big1} for the output to be minimized $\tilde{z}$,and C_{big2} and D_{big2} for the output to be controlled $\tilde{y}$ the following state equations for the infinite approximation of the augmented cantilever dynamics are obtained

$$\begin{aligned}
\dot{\hat{x}} &= A_{big}(S)\cdot\hat{x} + B_{big}\cdot\begin{bmatrix}\hat{w} & \hat{d} & r & u\end{bmatrix}' \\
\tilde{z} &= C_{big1}\cdot\hat{x} + D_{big1}\cdot\begin{bmatrix}\hat{w} & \hat{d} & r & u\end{bmatrix}' \\
\tilde{y} &= C_{big2}\cdot\hat{x} + D_{big2}\cdot\begin{bmatrix}\hat{w} & \hat{d} & r & u\end{bmatrix}'
\end{aligned} \tag{5.6}$$

Using the hinfsyn function of Matlab one obtains the state equations of the H_∞ controller:

$$\begin{aligned}
\dot{x}_k &= A_k(S)x_k + B_k(S)y \\
u &= C_k(S)x_k + D_k(S)y
\end{aligned}$$

Each of the matrices of the above equation of the controller can be written in the same manner as in equation 5.5. As an example the state matrix $A_k(S)$ with 3 neighbors on each side is presented

$$A_k(S) = A_{k-3}S^{-3}+A_{k-2}S^{-2}+A_{k-1}S^{-1}+A_{k0}+A_{k1}S^{1}+A_{k2}S^{2}+A_{k3}S^{3} \tag{5.7}$$

The coefficient matrices A_{ki} can be determined using Least Square Estimation (LSE). Let n denote the dimension of the matrix $A_k(S)$ and $A_k(i)$ the value of the operator $A_k(S)$ at the i_{th} gridding point of the Fourier frequency

θ

$$\begin{aligned} A_k(i) =&(I_n e^{-3j\theta}, I_n e^{-2j\theta}, I_n e^{-j\theta}, I_n, I_n e^{j\theta}, I_n e^{2j\theta}, I_n e^{3j\theta}) \\ &\times (A_{k-3}, A_{k-2}, A_{k-1}, A_{k0}, A_{k1}, A_{k2}, A_{k3})^* \\ :=&\psi_i \times \Omega \end{aligned} \tag{5.8}$$

In the above equation ψ_i can be easily calculated and $A_k(S) =$ is known. So for all the gridding points i the following equation can be written

$$\begin{bmatrix} A_k(1) \\ A_k(2) \\ \vdots \\ A_k(m) \end{bmatrix} = \begin{bmatrix} \psi_1 \\ \psi_2 \\ \vdots \\ \psi_m \end{bmatrix} \Omega$$

$$or \tag{5.9}$$

$$A_k = \Phi \times \Omega$$

where m is the number of the gridding points of Fourier frequencies θ. Using LSE theorem in [23], one of the best coefficient matrix estimates is given by

$$\Omega = [(Re\Phi)'(Re\Phi) + (Im\Phi)'(Im\Phi)]^{-1} \begin{bmatrix} Re\Phi \\ Im\Phi \end{bmatrix}' \begin{bmatrix} ReA_k \\ ImA_k \end{bmatrix} \tag{5.10}$$

with Re being the real part and Im being the imaginary part. The same calculations are done for $B_k(S)$, $C_k(S)$ and $D_k(S)$ and one obtains the distributed H_∞ controller

$$\begin{aligned} \dot{x}_k &= A_k x_k + B_k y_k \\ u_k &= C_k x_k + D_k y_k \end{aligned} \tag{5.11}$$

with the structure

$$\begin{aligned}\dot{x}_k =&[A_{k-3}S^{-3} + \ldots + A_{k0} + \ldots + A_{k3}S^3]x_k \\ &+ [B_{k-3}S^{-3} + \ldots + B_{k0} + \ldots + B_{k3}S^3]y_k \\ u_k =&[C_{k-3}S^{-3} + \ldots + C_{k0} + \ldots + C_{k3}S^3]x_k \\ &+ [D_{k-3}S^{-3} + \ldots + D_{k0} + \ldots + D_{k3}S^3]y_k\end{aligned} \tag{5.12}$$

or in matrix form

$$A_k = \begin{pmatrix} a_{k0} & a_{k1} & 0 & \cdots & 0 \\ a_{k1} & a_{k0} & a_{k1} & \cdots & 0 \\ \vdots & & \ddots & & 0 \\ 0 & \cdots & 0 & a_{k1} & a_{k0} \end{pmatrix} \tag{5.13}$$

In order to satisfy certain conditions for the H_∞ design and in order to have a small tracking error along with a low control effort the following weights are used: $W_u = 0.0025$, $W_{\hat{u}} = 2.3$, $W_w = 2.5$, $W_e = 32\frac{s+6000002}{s+0.0041}$, $W_{\hat{d}} = \frac{4}{s+100}$. The Bode plots of $W_{\hat{d}}$ and W_e can be seen in Figure 5.2 and Figure 5.1.

5.4 Simulation of the Nonlinear System

Results carried out in Matlab are presented in this section. The controller was tested on a model consisting of five cantilevers, same as the model for the centralized controller. However this time controller communicates only with the immediate neighbors and only receives current and voltage information from the cantilevers, unlike the feedforward and LQR controllers which contain the state information. So overall this is the controller having the least information from the system. The reference input has a frequency of 3000 rad/sec and a magnitude of 10 nm. The tracking error plot is presented in Figure 5.3. The absolute error is below 2 nm for all of the cantilevers and

it's around 1 nm for all of the cantilevers except for the ones at the edge. Figure 5.4 shows the comparison between the reference input and the tracked output for two sample cantilevers. These results are very similar to the results of the centralized controller presented in 4.5 and 4.6. This means, although having limited information the distributed H_∞ controller recovers the centralized control yields even better performance than the state feedback LQR controller at high frequencies as 3000 rad/sec. When the frequency of excitation is changed across the cantilever array the results in 5.5 and 5.6 are obtained that are not very different from 4.7 and 4.8 of the centralized H_∞ controller and better than 3.4 and 3.5 of the feedforward controller. So at varying frequencies the distributed H_∞ controller recovers the centralized H_∞ controller and is superior to the feedforward controller. Figure 5.7 presents the control effort that is less than 4 V, implying that the distributed H_∞ controller requires less effort than the feedforward and LQR controllers.

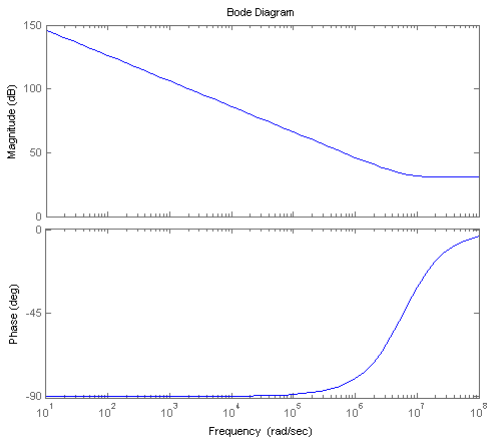

Figure 5.1: Bode Plot for W_e

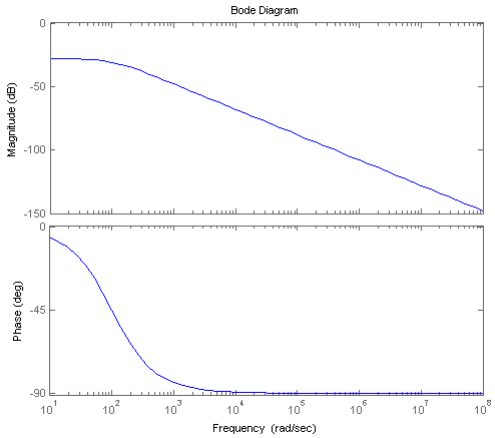

Figure 5.2: Bode Plot for W_d

5.5 Stability and Robustness Analysis

Stability analysis of the closed loop distributed H_∞ control system is performed in this section. Figure 5.8 presents the sensitivity plot of the system that has a bandwidth close to 40000 rad/sec. So the feedback is effective in a wider region than the feedforward and LQR controllers and the performance of the centralized controller is almost recovered. This is also verified by the LSTI infinite abstraction of the system in Figure 5.9. The very similar result of the LSTI plot to the sensitivity plot of the five cantilever system also implies that the simulation results of the previous section are a good representation of the actual system with a large number of cantilevers. Furthermore the simulations also show that the system does not get unstable even at very high excitation frequencies. The tracking error is around 2 nm at 6000 rad/sec and increases further as the frequency gets higher but the system is still stable at frequencies as high as 30000 rad/sec.

As in chapter 3 for the state feedback controllers, the phase and gain margins are calculated also for the output feedback H_∞ control that is im-

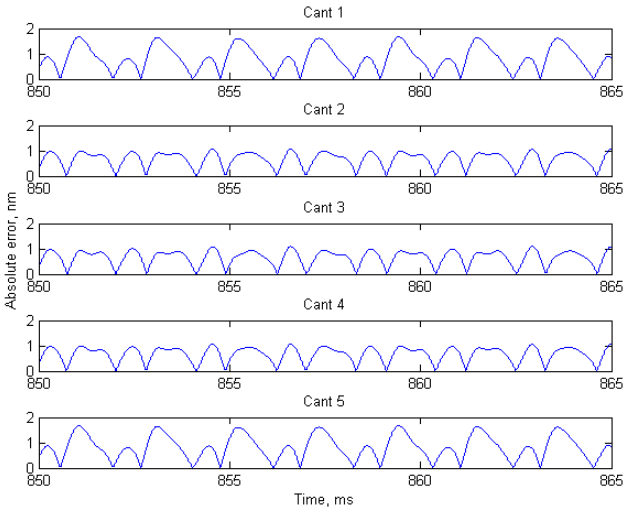

Figure 5.3: Distributed H_∞ Control design: Tracking error of 5 cantilevers at the excitation frequency of 3000 rad/sec and 10 nm amplitude

plemented on the isolated single cantilever. The system with the controller has a phase margin of 60.4 degrees and a gain margin of 11.1 dB, as shown in Figure 5.10. The closed loop system is stable and both margins have more desirable values than the feedforward controller. This result is compatible with the relatively low peak value of the sensitivity plot of the closed loop system presented in Figure 5.8 indicating the high robustness of the system.

For further robustness analysis of the distributed H_∞ control the structured singular value (SSV) is calculated, both for the finite 5 cantilever system and for the infinite abstraction. The same uncertainty structure with the same gains is used as described in equations 3.13 and 3.15. The plots can be seen in Figure 5.11 and Figure 5.12 for the finite and infinite models respectively. The magnitude of the SSV is very close to the SSV of the centralized H_∞ control. This implies that the robust performance properties of the centralized controller can be achieved by the distributed controller.

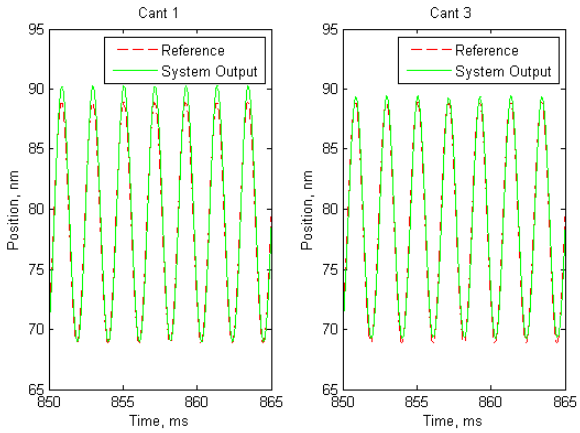

Figure 5.4: Distributed H_∞ Control design: Reference input and tracked output for two sample cantilevers with the excitation frequency and amplitude being 3000 rad/sec and 10 nm respectively

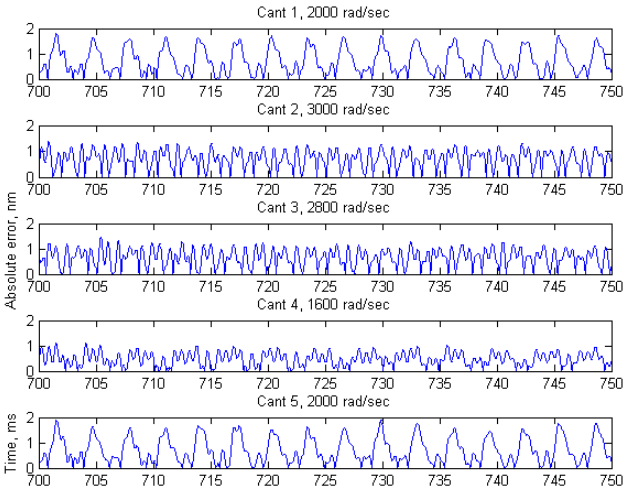

Figure 5.5: Distributed H_∞ Control design: Tracking error of 5 cantilevers at different excitation frequencies

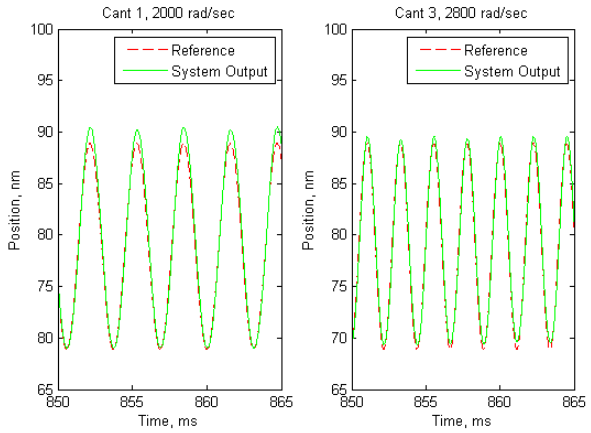

Figure 5.6: Distributed H_∞ Control design: Reference input and tracked output for 2 sample cantilevers at different excitation frequencies

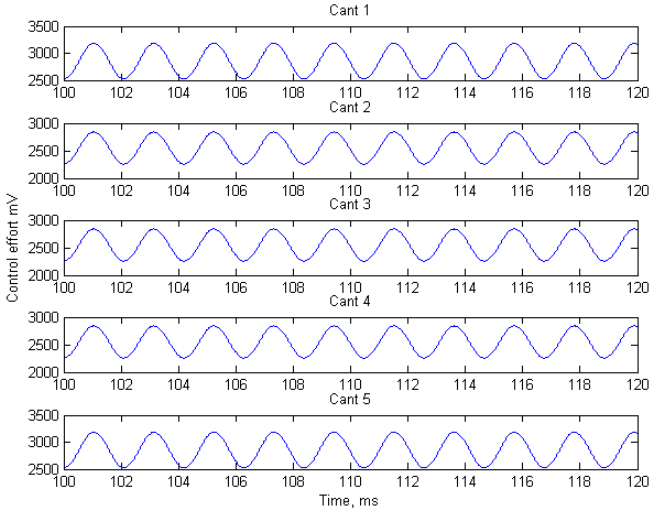

Figure 5.7: Distributed H_∞ Control design: Control Effort of the cantilevers in a 5 cantilever system. The excitation frequency and amplitude are 3000rad/sec and 10nm respectively

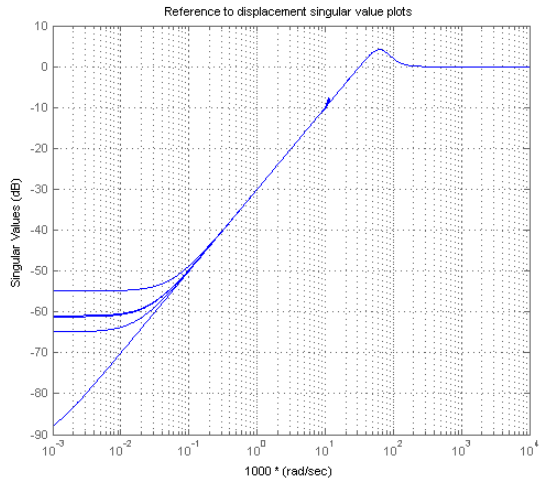

Figure 5.8: Sensitivity Plot of the Distributed H_∞ Control System

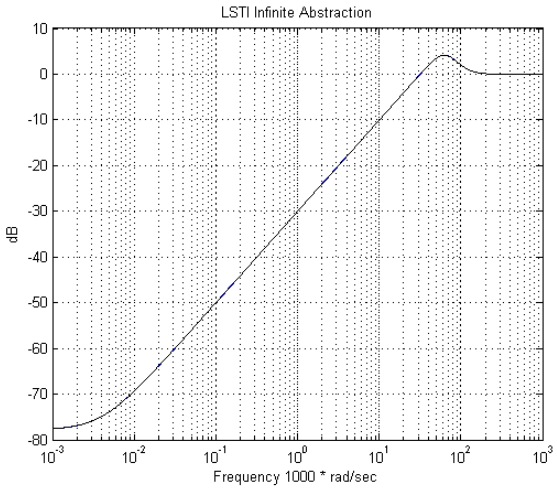

Figure 5.9: LSTI infinite abstraction Bode magnitude plot of reference to error transfer function for one cantilever using distributed H_∞ Control

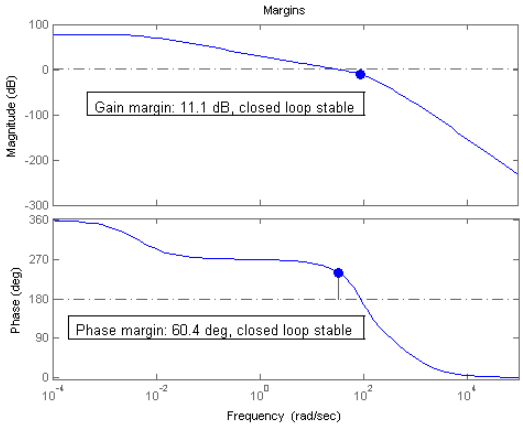

Figure 5.10: Phase and gain margins of the H_∞ Control System for an isolated cantilever

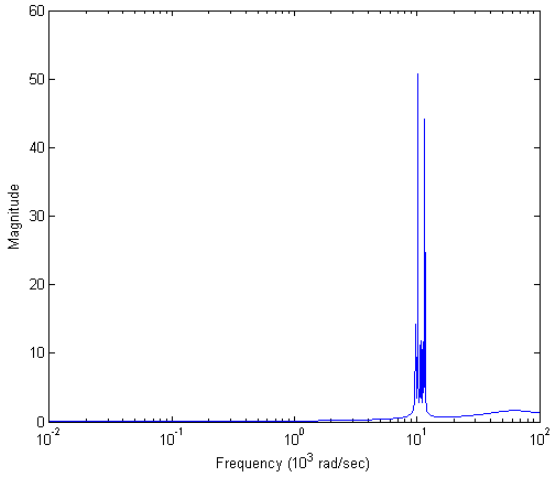

Figure 5.11: Structured singular value plot for the closed loop system of 5 cantilevers with the distributed H_∞ control

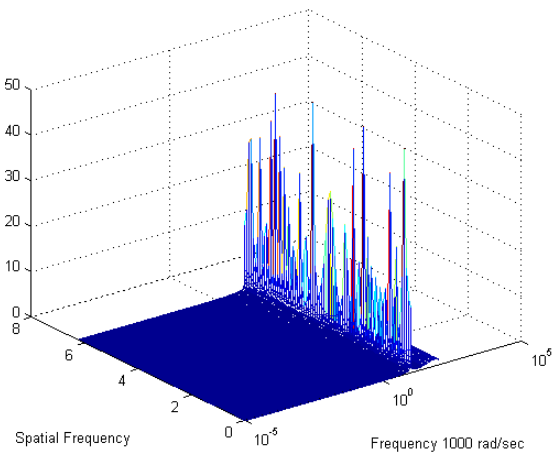

Figure 5.12: Structured singular value plot for the closed loop system with the distributed H_∞ control designed using infinite abstraction

CHAPTER 6

MULTIMODAL MODEL

6.1 Introduction

The performance and robustness analysis with various controllers was done so far with a simplified model of the cantilever array where each cantilever was observed as one dynamical unit having only 3 states, namely its position, velocity and the voltage applied on it. However in reality the cantilever is not a point mass but has a more complicated structure instead. Therefore in order to have a more accurate analysis on the control performance the further complexities of the cantilever system have to be taken into account. Multimodal modeling, or finite element method particularly, cuts the structure into several elements, creates dynamical equations for each element and describes the equations of a single cantilever by combining them.

6.2 Finite Element Method

As shown in Figure 6.1 each cantilever is assumed to consist of n beam elements, resulting in $n+1$ position points. Each position point has a vertical displacement and also a rotation of the beam at the point associated with it.

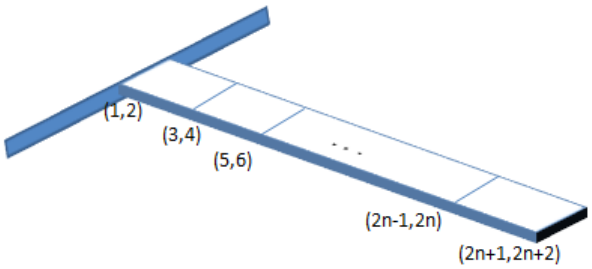

Figure 6.1: Multimodal model of the cantilever beam

Thus each cantilever has $2 \cdot (n+1)$ states:

$$\bar{z}_i = \begin{bmatrix} x_{i,v,1} \\ x_{i,\theta,1} \\ x_{i,v,2} \\ x_{i,\theta,2} \\ \vdots \\ x_{i,v,n+1} \\ x_{i,\theta,n+1} \end{bmatrix} \tag{6.1}$$

The FEM model uses a base matrix for each beam element with

$$K_1 = \frac{EI}{h^3} \cdot \begin{bmatrix} 12 & 6h & -12 & 6h \\ 6h & 4h^2 & -6h & 2h^2 \\ -12 & -6h & 12 & -6h \\ 6h & 2h^2 & -6h & 4h^2 \end{bmatrix} \tag{6.2}$$

as the base stiffness matrix and

$$M_1 = \frac{\rho A_r h}{420} \cdot \begin{bmatrix} 156 & 22h & 54 & -13h \\ 22h & 4h^2 & 13h & -3h^2 \\ 54 & 13h & 156 & -22h \\ -13h & -3h^2 & -22h & 4h^2 \end{bmatrix} \tag{6.3}$$

as the base mass matrix. These matrices are derived from the principal of virtual work by assuming a cubic interpolation function for the displacements. E signifies the Young's modulus, I the area moment of inertia about the z-axis, h the element length ρ the density and A_r the cross-section area. The matrices in 6.2 and 6.3 are used to produce the beam mass matrix M and beam stiffness matrix K for each cantilever. These are created in a pattern where the base submatrix is placed in the top left corner and the next submatrix is placed diagonal to the previous location, shifted two down and two across. The pattern of the beam stiffness matrix K is shown in 6.4

$$K = \begin{bmatrix} k_1 & k_1 & k_1 & k_1 & 0 & \dots & & & & \\ k_1 & k_1 & k_1 & k_1 & 0 & & & & & \\ k_1 & k_1 & k_1+k_2 & k_1+k_2 & k_2 & & & & & \\ k_1 & k_1 & k_1+k_2 & k_1+k_2 & k_2 & & & & & \\ 0 & 0 & k_2 & k_2 & k_2+k_3 & & & & & \\ \vdots & & & & & \ddots & & & & \\ 0 & & & & & & k_{n-1}+k_n & k_{n-1}+k_n & k_n & k_n \\ 0 & & & & & & k_{n-1}+k_n & k_{n-1}+k_n & k_n & k_n \\ 0 & & & & & & k_n & k_n & k_n & k_n \\ 0 & & & & & & k_n & k_n & k_n & k_n \end{bmatrix} \tag{6.4}$$

where k_i is the element of the base matrix of the $i'th$ beam element and each cantilever has n beam elements. The beam mass matrix M has the same structure. The M and K matrices are used in the basic characteristic equation of the form:

$$M\ddot{x} = -Kx \tag{6.5}$$

The mass matrix can be moved to the other side to give us the solution to cantilever system

$$\ddot{x} = -M^{-1}Kx = (M\_K)x \tag{6.6}$$

where M_K is a $(2n+2) \times (2n+2)$ single mass-stiffness matrix for one cantilever. To make sure the attached end of the cantilever is rigid the first and second rows and columns are zeroed, meaning that the cantilever position at the attached end cannot change. The obtained M_K matrix is used in the modified characteristic equation of the cantilever system.

Because $\hat{x}_{i,1}$ of the i_{th} cantilever is measured at the tip the vertical displacement of the last beam element and the corresponding velocity are used for coupling calculations and the calculation of the current: $\hat{x}_{i,1} = x_{i,v,n+1} = \bar{z}_i(2n+1)$ and $\hat{x}_{i,2} = \dot{x}_{i,v,n+1} = \dot{\bar{z}}_i(2n+1)$. Assuming the equilibrium values of $\bar{z}_i$, $\dot{\bar{z}}_i$ and V_i given by $\bar{z}_e$, 0, V_e respectively the following definitions are made: $\bar{x}_{1i} = \bar{z}_i - \bar{z}_e$, $\bar{x}_{2i} = \dot{\bar{z}}_i$, $\bar{x}_{3i} = V_i - Ve$. The modified state space equations of the multimodal cantilever can now be written:

$$\begin{aligned}
\dot{\bar{x}}_{1i} &= \bar{x}_{2i} \\
\dot{\bar{x}}_{2i} &= (M_K)\bar{x}_{1i} - b\bar{x}_{2i} + F_{tot,i}P \\
\dot{\bar{x}}_{3i} &= u
\end{aligned} \tag{6.7}$$

where P is a $(2n+2) \times 1$ vector with $P(2n+1) = 1$ and the other elements of the vector being 0. $F_{tot,i}$ is the sum of all the forces acting on the $i'th$ cantilever:

$$F_{tot,i} = F_{a,i} + F_{mech,i} + F^{\perp}_{elec,i} \tag{6.8}$$

6.2.1 Linearization

As in the simple model the equilibrium position is calculated as follows:

$$\begin{aligned}
\dot{\bar{x}}_{1i} &= \bar{x}_{2i} = 0 \\
\dot{\bar{x}}_{2i} &= (M_K)\bar{x}_{1i} - b\bar{x}_{2i} + F_{tot,i}P = 0 \\
\dot{\bar{x}}_{3i} &= u = 0
\end{aligned} \tag{6.9}$$

Where

$$\begin{aligned}
F^e_{a,i} &= \frac{\epsilon_0 A}{2md^2}(1 + \frac{2x_{e1}}{d})V_e^2 \\
F^e_{mech,i} &= 0 \\
F^{e\perp}_{elec,i} &= 0
\end{aligned} \tag{6.10}$$

Thus one needs to solve the following equation:

$$(M\_K)\bar{x}_{1i} + F^e_{a,i} = 0 \tag{6.11}$$

In the linearization of the simple nonlinear model and equilibrium voltage of 5.5 Volts was used. If this value is put into 6.11 one calculates the equilibrium displacement of the cantilever tip, namely $x_{i,v,n+1}$, to be 0.0181 micrometers. The corresponding singular value plot of the reference to tip displacement transfer function of the open loop system is depicted in Figure 6.2. In the frequency range of interest, which is around 1000-3000 rad/sec or less, there is an offset between the singular value plot of the open loop transfer function of the simple system and the singular value plot of the FEM system. The offset can be removed by increasing the equilibrium voltage. In Figure 6.3 you see the singular value plots of the FEM model and simple model for an equilibrium voltage of 17.625 Volts. The singular value plot of the FEM model shifted upwards towards the singular value plot of the simple model, resulting in similar frequency response plots for both open loop systems for

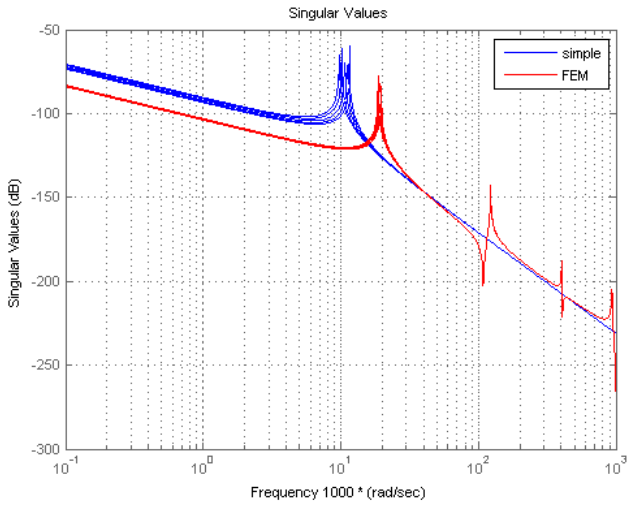

Figure 6.2: Comparison of the open loop transfer functions of the simple model and FEM, with the equilibrium voltage being 5.5 V

the frequency range of interest. The corresponding equilibrium tip position is 0.224 micrometers.

The linearization results show that with the redefined equilibrium values, the same controllers as in the simple nonlinear model can be used for the more complicated multimodal system. In the following sections the simulation results of the system with the feedforward controller, LQR controller and the H_∞ controllers are explained.

6.3 Feedforward Control for FEM

In this section the same feedforward controller is used as in Chapter 3. The controller is decentralized and is not using any information from the neighbors. However the displacement information of the cantilever is provided. The system's being more complicated causes longer calculation and simulation times. Therefore a cantilever model of 5 cantilevers is tested. In order to further reduce the complexity it is assumed that each cantilever has only

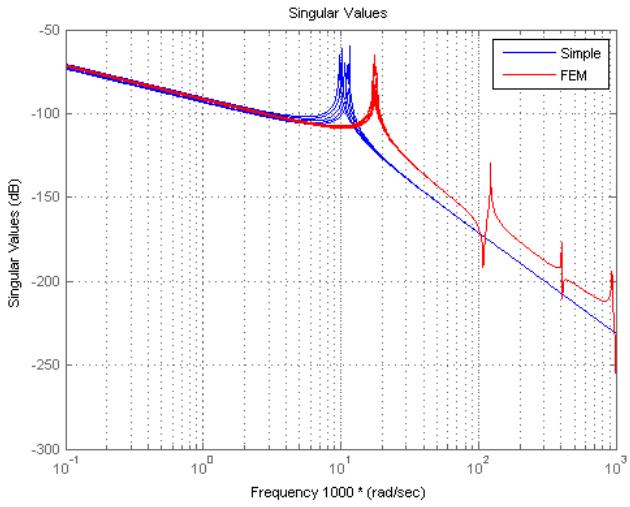

Figure 6.3: Comparison of the open loop transfer functions of the simple model and FEM, with the equilibrium voltage being 17.625 V

2 beam elements. The reference frequency is also lowered from 3000 rad/sec to 1000 rad/sec, however the amplitude is the same, namely 10 nm.

Figure 6.4 shows the absolute tracking error of the 5 cantilevers of the nonlinear system. The error is clearly less than 1 nm for all of the cantilevers. So although the system dynamics are different from the simple model the controller yields a good performance. The tracking performance is depicted in Figure 6.5 where the displacement of 2 sample cantilevers is compared with the reference input.

The tracking results of Figure 6.4 are obtained at the expense of high control effort. As seen in Figure 6.6 the voltage applied on the cantilever reaches 19.5 V, that is much higher than the control effort required for the simple model.

The good tracking results can also be shown in frequency domain. Figure 6.7 compares the closed loop singular value plots of the reference to displacement transfer functions of 2 models. The bandwidth is larger than

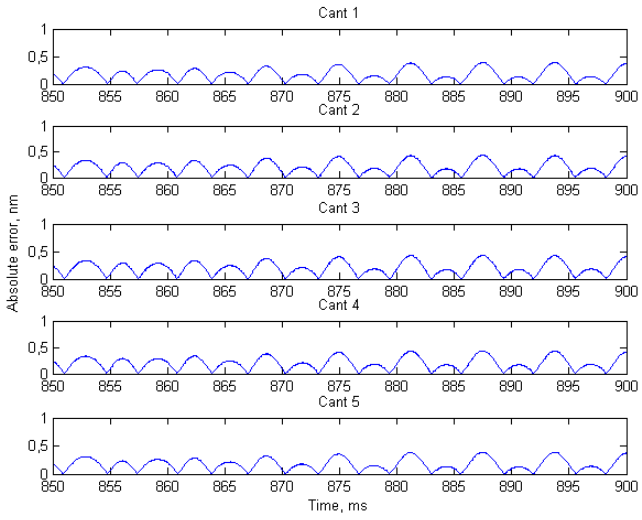

Figure 6.4: Feedforward Control design: Tracking error of 5 cantilevers of the nonlinear system. The excitation frequency is 1000 rad/sec and the amplitude is 10 nm

1000 rad/sec and in the frequency region of interest, where 1000 rad/sec is included, the singular value plots match together, verifying the tracking results in time domain.

6.4 LQR Control for FEM

In this section the LQR controller introduced in Chapter 3 is implemented on the nonlinear FEM model with the new equilibrium values. Each cantilever has its own controller that communicates with immediate neighbors only and has the state information from the cantilever. The model consists of 5 cantilevers and the reference input has a frequency of 1000 rad/sec and a magnitude of 10 nm, shifted by the new defined equilibrium value of 0.224 nm.

Figure 6.8 shows the absolute tracking error of the 5 cantilevers of the nonlinear system. With an absolute tracking error of around 1 nm the LQR

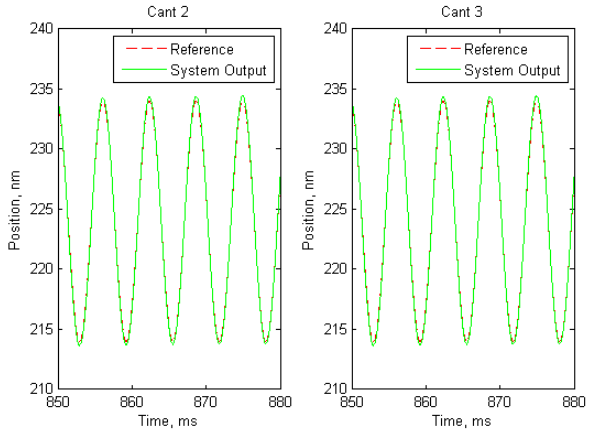

Figure 6.5: Feedforward Control design: Reference input and tracked output for two sample cantilevers of the nonlinear system. The excitation frequency and amplitude are 1000rad/sec and 10nm respectively

controller provides good performance for the FEM model although being designed for the simple model. Figure 6.9 shows the comparison of the tracked output to the reference input for 2 cantilevers as an example. The payoff of the good tracking performance is the high control effort that is around 17.5 V as seen in Figure 6.10. This value is much higher than the control effort required by the simple model.

Finally frequency domain analysis is conducted for the closed loop system with FEM modeling. Figure 6.11 shows the complementary sensitivity functions of both the simple and the FEM models. At frequencies below 5000 rad/sec both plots match, and their bandwidth is above 5000 rad/sec, verifying the simulation results.

6.5 H_∞ Control

It has been shown that with changing the equilibrium values frequency response similar to the simple system can be obtained for the FEM system, which is further verified by simulation results with state feedback controllers.

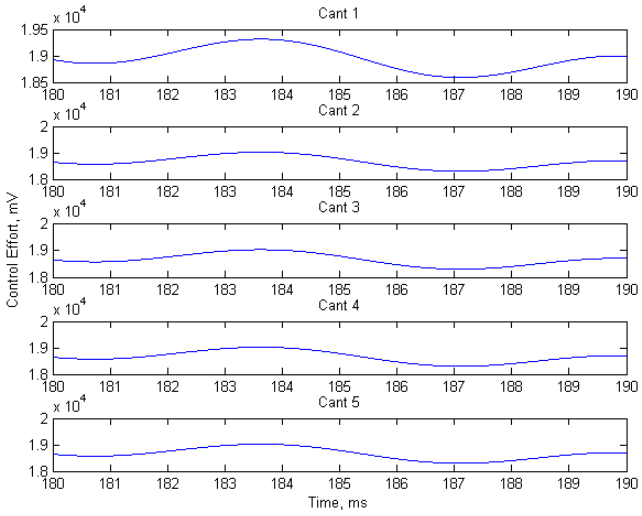

Figure 6.6: Sample control effort for five cantilever FEM system with the feedforward control. The excitation frequency and amplitude are 1000rad/sec and 10nm respectively

This means that the H_∞ controller that is designed for the simple system may be used for the more complicated multimodal cantilever design. This is a significant advantage for the control design process since it reduces the amount of calculations. A cantilever with n beam elements has $n+1$ position points and each position point has 2 position and 2 velocity states. In addition to these there is the state corresponding to the control effort. So in total, for a cantilever beam consisting of only 2 beam elements there are 13 states which is too high in comparison to 3 states for the simple model. A new H_∞ controller designed for this system would have 15 states if the same weights were introduced as in the previous chapters, resulting in $13 + 15 + 1 = 29$ states for just one cantilever. The H_∞ controller designed from the simple system only has 5 states, resulting in $13 + 5 + 1 = 19$ states if used for the FEM system.

Firstly the centralized H_∞ controller from Chapter 4 is implemented to the

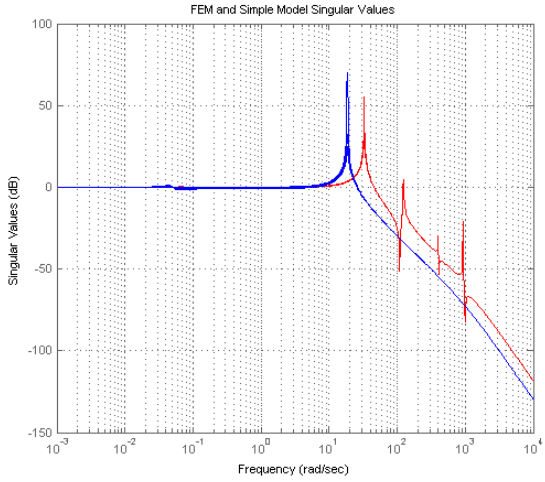

Figure 6.7: Reference to displacement singular value plot of the closed loop systems of simple model and FEM. Feedforward controller is used

nonlinear FEM system, consisting of 5 cantilevers. So as in Chapter 4 the controller receives all the output and coupling information from the system and it has 25 states. Simulations are done with a reference input having a frequency of 1000 rad/sec and a magnitude of 10 nm. Figure 6.12 shows the absolute tracking error of 5 cantilevers. Except for a local degradation in the edge cantilevers the centralized controller yields satisfactory tracking performance with an absolute error around 1 nm. The comparison of the reference input with the tracked output of 2 sample cantilevers is depicted in Figure 6.13. According to further simulations the tracking error increases up to 2 nm at 3000 rad/sec and 5 nm at 6000 rad/sec. However the system is stable at frequencies as high as 30000 rad/sec.

Obviously the good performance of the centralized controller, that is designed for the simple linearized system and used for the multimodal nonlinear system, has some payoffs. A clear evidence for this is the control effort presented in Figure 6.14. Similar to the observations from the feedforward and

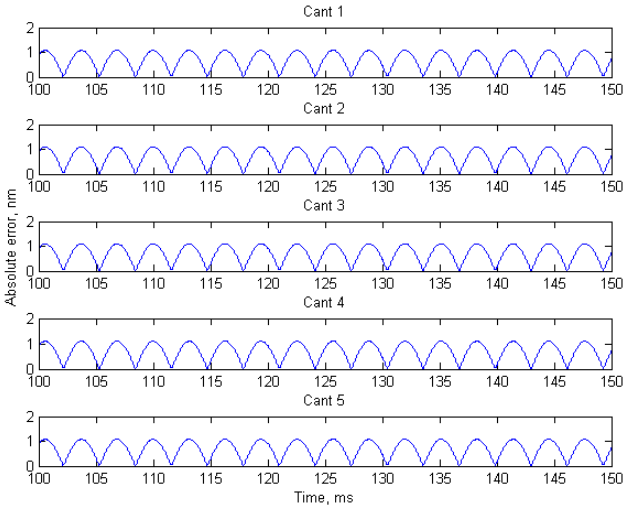

Figure 6.8: LQR Control design: Tracking error of 5 cantilevers of the nonlinear system. The excitation frequency is 1000 rad/sec and the amplitude is 10 nm

LQR controllers, the required control effort is much higher than in the simple model and goes up to 14.5 V.

A comparison between the simple and multimodal models in the frequency domain with the centralized H_∞ controller is now presented. Figure 6.15 shows the complementary sensitivity functions for both types of modeling. At frequencies lower than 5000 rad/sec the plots of both models match however after that point the multimodal model starts to deteriorate having high peak values. This observation implies that the centralized H_∞ control developed in Chapter 4 could be an acceptable controller at frequencies lower than 5000 rad/sec for the multimodal system and should provide a benchmark for the distributed H_∞ control of Chapter 5.

Once having defined the benchmark for the distributed H_∞ control its implementation on the multimodal FEM model is analyzed in the next step. The same controller as in Chapter 5 is tested on the FEM model of 5 can-

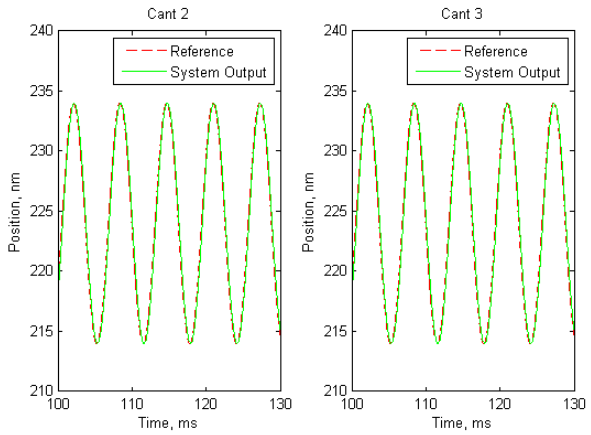

Figure 6.9: LQR Control design: Reference input and tracked output for two sample cantilevers of the nonlinear system. The excitation frequency and amplitude are 1000rad/sec and 10nm respectively

tilevers. Each controller is in communication with only two of its neighbors (one on each side) while the first and the fifth controllers (the ones at the edge) are truncated such that no information is passed to them from their neighbors. The reference frequency is 1000 rad/sec and the reference magnitude is 10 nm. Figure 6.16 shows the absolute tracking error of 5 cantilevers of the nonlinear system. The same phenomena of performance degradation at the edge cantilevers is observed with the distributed H_∞, too. The absolute error is close to 10 nm in this case. However the absolute tracking error of the cantilevers in between is less than 2 nm which is an acceptable result. The tracking performance is depicted in Figure 6.17 where the displacement of 2 sample cantilevers is compared with the reference input.

Similar to the centralized controller, the distributed H_∞ control requires a control effort with of approximately 14.5 V for the FEM design as depicted in Figure 6.18, much higher than the voltage calculated for the simple model.

Finally the above tracking results can also be shown in frequency domain. Figure 6.19 compares the closed loop singular value plots of the reference to

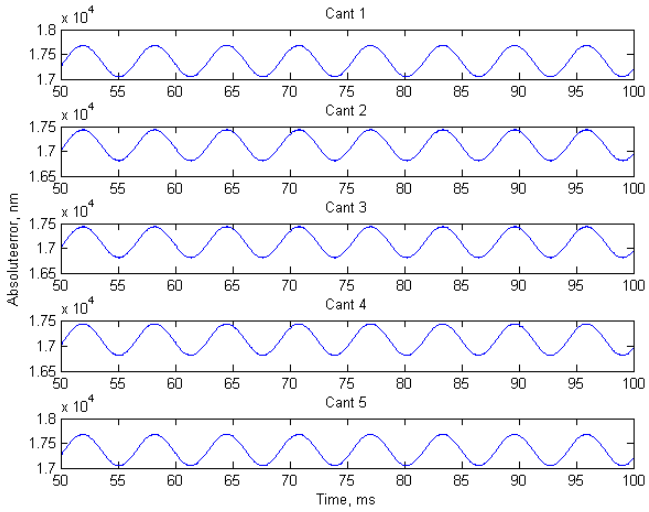

Figure 6.10: Sample control effort for five cantilever FEM system with the LQR control. The excitation frequency and amplitude are 1000rad/sec and 10nm respectively

displacement transfer functions of 2 models. The bandwidth is larger than 1000 rad/sec and in the frequency region of interest, where 1000 rad/sec is included, the singular value plots match together, verifying the tracking results in time domain.

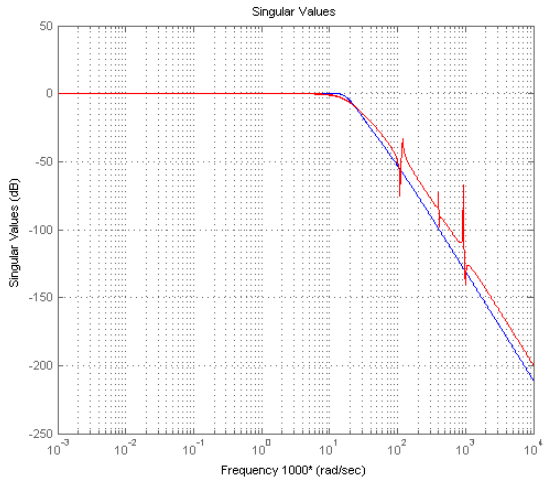

Figure 6.11: Reference to displacement singular value plot of the closed loop systems of simple model and FEM. The LQR controller is used

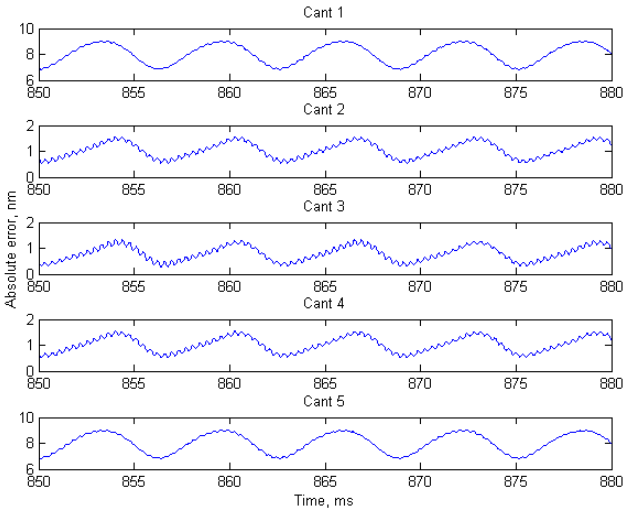

Figure 6.12: Centralized H_∞ Control design: Tracking error of 5 cantilevers of the FEM system. The excitation frequency and amplitude are 1000rad/sec and 10nm respectively

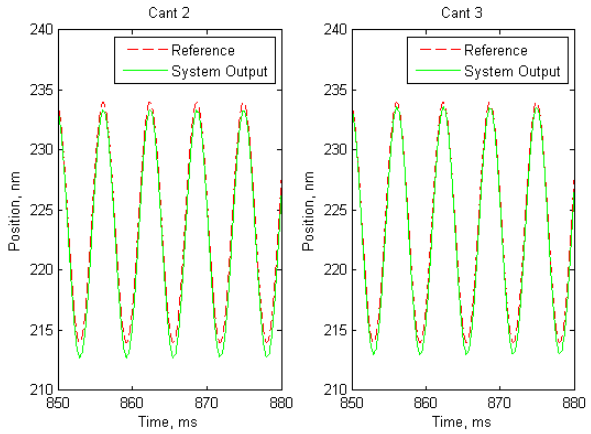

Figure 6.13: Centralized H_∞ Control design: Reference input and tracked output for two sample cantilevers of the nonlinear system. The excitation frequency and amplitude are 1000rad/sec and 10nm respectively

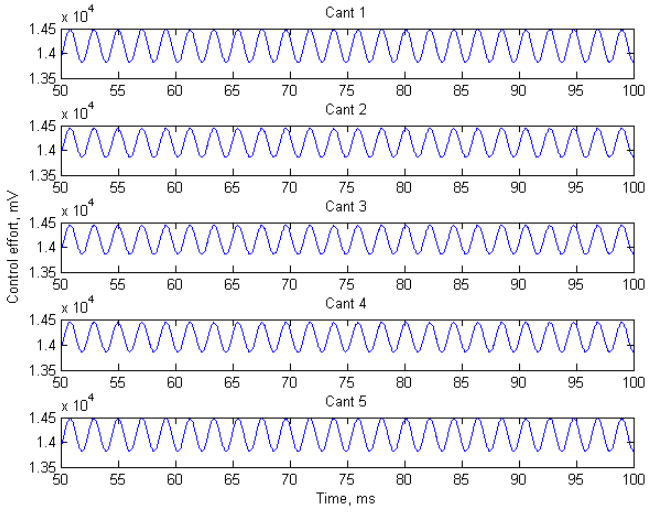

Figure 6.14: Sample control effort for five cantilever FEM system with the LQR control. The excitation frequency and amplitude are 1000rad/sec and 10nm respectively

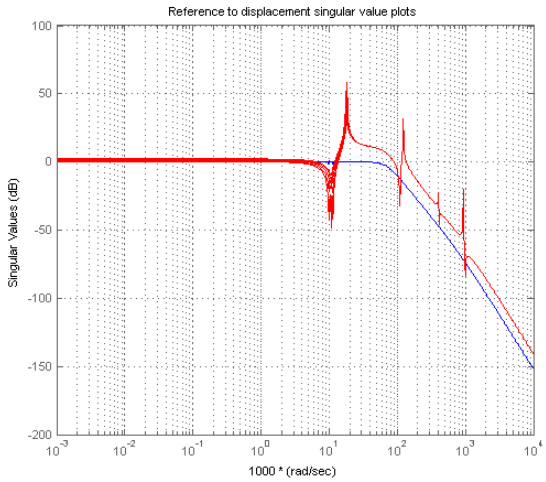

Figure 6.15: Reference to displacement singular value plot of the closed loop systems of simple model and FEM. Centralized H_∞ controller is used

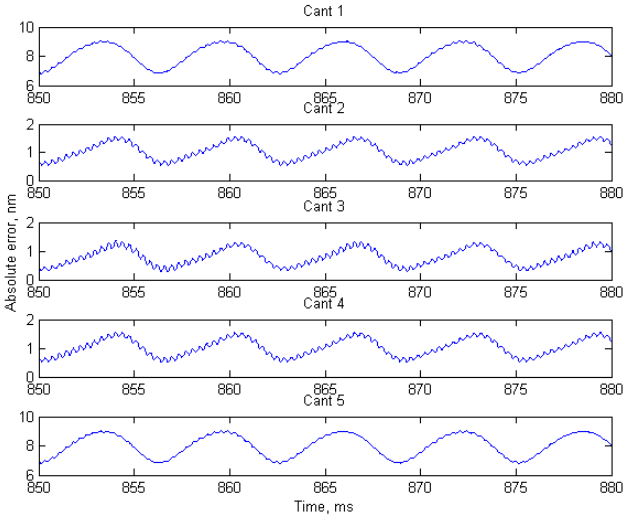

Figure 6.16: Distributed H_∞ Control design: Tracking error of 5 cantilevers of the nonlinear FEM system with the excitation frequency and amplitude being 1000 rad/sec and 10 nm respectively

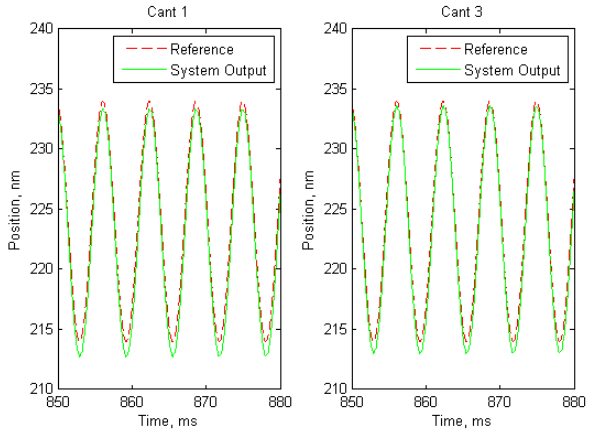

Figure 6.17: Distributed H_∞ Control design: Reference input and tracked output for two sample cantilevers of the nonlinear FEM system. The excitation frequency and amplitude are 1000rad/sec and 10nm respectively

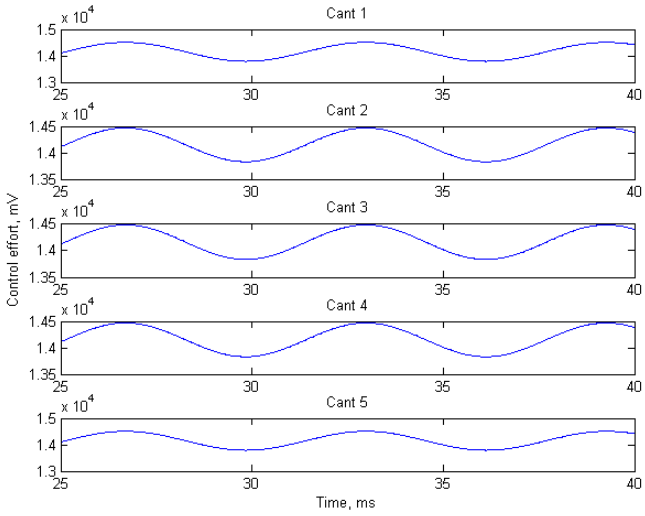

Figure 6.18: Sample control effort for five cantilever FEM system with the H_∞ control at the excitation frequency of 1000 rad/sec

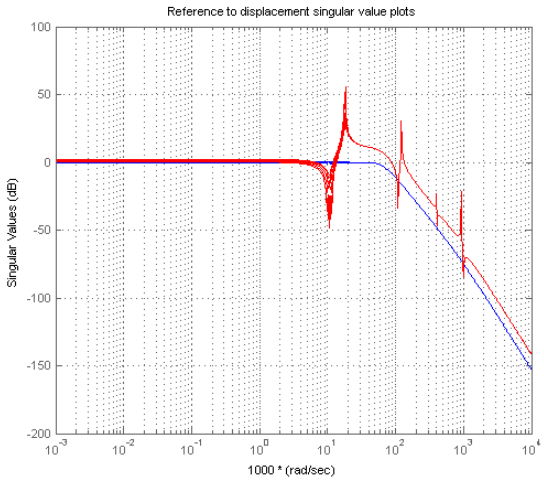

Figure 6.19: Reference to displacement singular value plot of the closed loop systems of simple model and FEM. Distributed H_∞ controller is used

CHAPTER 7

CONCLUSIONS

In this thesis the modeling and control of an infinite array of electrostatically actuated microcantilevers has been presented. The cantilevers have weak mechanical and electrostatic couplings where only 3-4 neighbors on each side make any significant contribution. Furthermore the dynamics of the cantilevers do not change along a spatial axis, meaning that the system is spatially invariant.

The modeling of the cantilever was performed in 2 different ways. The first one was a simple nonlinear model where each cantilever was considered as a point mass with its displacement, velocity and voltage being the only states, whereas the second one was a multimodal model that considered each cantilever as a more complex structure consisting of smaller segments each having rotational and vertical displacements and velocities as their states. For the successful actuation of the cantilevers 2 types of controllers were developed and implemented, the first type being the state feedback and the second type being the output feedback. All of the controllers were designed from the linearization of the simple nonlinear model.

The first state feedback controller is a PID controller having additionally a velocity feedforward component from the reference. It is a fully decentralized controller and designed by adjusting the weights for the best performance. Although it yields a resolution of less than 1 nm at frequencies as high as 3000 nm for the simple nonlinear model, given that the same excitation fre-

quency is used across the array, the tracking error may increase up to 10 nm if the excitation frequency is changed. Frequency analysis and simulations furthermore indicate that the tracking performance may deteriorate at higher frequencies. Because of these downsides of the feedforward controller the optimal state feedback controller from [22] was introduced next. The LQR type controller, that was designed by simultaneous localization and optimization, has a distributed structure where each controller communicates with the immediate neighbors only. This controller is robust in comparison to the feedforward controller and yields acceptable results at excitation frequencies up to 2000 rad/sec according to the simulations with the simple nonlinear model, even if the frequency is varied across the array. However it does not provide enough resolution at higher frequencies.

The analysis with the FEM model also verified the above results, although due to the increased control effort the feedforward controller may still yield an acceptable performance at frequencies higher than 4000 rad/sec. The state feedback controllers hence may be a vital alternative in cases where the excitation frequencies are not too high or they do not vary significantly across the array and when the state information is available. In more general cases, however, the output feedback H_∞ controller is more suitable for the high density microcantilever array system, as demonstrated in this thesis. Firstly a centralized, output feedback H_∞ controller was introduced for a finite number of cantilevers. The centralized controller is not applicable on large array systems because of its complexity and therefore it yields a benchmark for the distributed H_∞ control, with a tracking error less than 2 nm at the excitation frequency of 3000 rad/sec, low tracking errors at varying frequencies and higher frequency bandwidths than the state feedback controllers. The distributed controller, localized for each cantilever and

communicating only with immediate neighbors, can attain the performance of the centralized control in terms of tracking, stability at higher frequencies and robustness. This result can also be observed in the analysis with the FEM model, where except for the edge cantilevers, which can be neglected from an operational point of view, the tracking error remains below 2 nm for both the centralized and the distributed controllers; however at the expense of higher control effort and lower bandwidth of the sensitivity function.

In conclusion, the state feedback controllers with the feedforward or LQR structures may be significant alternatives for the high density cantilever array. Their implementation is not complicated, require less calculation time and provide satisfactory results. However the distributed H_∞ controller is the most appropriate one for spatially and temporally invariant array systems especially when the states are not measurable. Future work can be directed towards more comprehensive robustness analysis, experiments with the existing controllers and further investigation of the LQR control from [22].

REFERENCES

[1] M. Sitti., "Micro and Nano-Scale Robotics", *American Control Conference*, Boston, MA, July 2004

[2] F.J. Giessibl, "Advances in Atomic Force Microscopy", *Rev. of Modern Physics*, vol. 75,no. 3, pp. 950-983, July 2003.

[3] A.M. Moulin, S.J. O'Shea, and M.E. Welland, "Microcantilever-based biosensors", *Ultramicroscopy*, vol. 82, no. 1-4, pp. 23-31, February 2000.

[4] R. Garcia, and R. Perez, "Dynamic Atomic Force Microscopy Methods", *Surface Science Reports*, vol. 47, pp. 197-301, 2002

[5] W. Zhou, A. Khaliq, Y. Tang, H. Ji, and R. Selmic, "Simulation and design of piezoelectric microcantilever chemical sensors", *Sensors and Actuators A: Physical*, vol. 125, no. 1,21, pp. 69-75, October 2005.

[6] E. A. Wachter, T. Thunat, P.I. Oden, R.J. Warmack, P.G. Datskos, and S.L. Sharp, "Remote optical detection using microcantilevers", *Review of Scientific Instruments*, vol. 67, no. 10, 1996.

[7] M. Despont, J. Brugger, U. Drechsler, U. Durig, W. Haberle, M. Lutwyche, H. Rothuizen, R. Stutz, R. Widmer, G. Binning, H. Rohrer, and P. Vettiger, "VLSI-NEMS chip for parallel AFM data storage", *Sensors and Actuators A: Physical*, vol. 80, no. 2,10, pp. 100-107, March 2000.

[8] A. Sarwar, P.G. Voulgaris, and S.M. Salapaka "On the control design and robustness analysis for high-density microcantilever arrays", *Journal of Vibration and Control*, vol. 17, no. 8, pp. 1195-1210 July 2011

[9] A. Sarwar, "Modelling and Control of Electrostatically Actuated Microcantilever Array", M.S. thesis, University of Illinois at Urbana-Champaign, Urbana, IL, 2006.

[10] M. Napoli, "Modelling and control of electrostatically actuated microcantilever arrays", Ph. D. dissertation, University of California at Santa Barbara, Santa Barbara, CA, 2004.

[11] M. Napoli, B. Bamieh, "Design of a Decoupling Controller for electrostatically Coupled Microcantilevers Based on Current Measurement", *American Control Conference, 2004. Proceedings of the 2004*, vol. 4, pp. 3134-3139, June-July 2004.

[12] E. Volterra, E.C. Zachmanoglou, *Dynamics of Vibrations*, Colombus, Ohio: C.E. Merrill Books, 1965.

[13] G. Sauer, and M. Wolf, "A Modified Beam Element Mass Matrix", *Zeitschrift für angewandte Mathematik und Mechanik*, vol. 68, no. 10, pp. 483-490, 1988.

[14] M. Napoli, W. Zhang, B. Bamieh, and K. Turner, "Dynamics of Mechanically and Electrostatically Coupled Microcantilevers" *International Conference on Transducers, Solid-State Sensors, Actuators and Microsystems*, vol. 2, pp. 1088-1091, June 2003.

[15] M. Napoli, B. Bamieh, and K. Turner, "A capacitive microcantilever: Modeling, validaton and estimation using current measurements." *ASME*

Journal of Dynamical Systems Measurement and Control, vol. 126, pp. 319-326, June 2004.

[16] K. Ogata, "System Dynamics", *Pearson Prentice Hall*, Upper Saddle River, NJ, 2004

[17] Zhou, K., J.C. Doyle, and K. Glover, "Robust and Optimal Control", *Prentice Hall*, Inc. 1996.

[18] Skogestad, S. and I. Postlethwaite, "Multivariable Feedback Control-Analysis and Design", *John Wiley and Sons*, Inc. 1996.

[19] B. Bamieh, F. Paganini, and M.A. Dahleh, "Distributed Control of spatially invariant systems", *IEEE Transactions on Automatic Control*, vol. 47, no. 7, pp. 1091-1107, July 2002

[20] D. Gorinevsky and G. Stein, "Structured Uncertainity Analysis of Robust Stability for Multidimensional Array Systems"*IEEE Transaction on Automatic Control*, vol. 48, pp. 1557-1568, 2003

[21] G. Stein and D. Gorinevsky, "Design of Surface Shape Control for Large Two-Dimensional Arrays" *IEEE Transaction on Control Systems Technology*, vol. 13, 2005

[22] F. Lin, M. Fardad, and M. R. Jovanovic, "Augmented Lagrangian approach to design of structured optimal state feedback gains" *IEEE Transactions on Automatic Control*, vol. 56, no.12, December 2011

[23] Ljung L., "System Identification: Theory for the User" *Prentice Hall*, Inc. 1987

[24] Dullerud, G.E. and F. Paganini, "A Course in Robust Control Theory-A Convex Approach", *Springer Verlag*, Inc. 2000.

[25] Curtain, R. F. and H. J. Zwart, "An Introduction to Infinite Dimensional Linear System Theory", *Springer Verlag*, Inc. 1995.